NASA TECHNICAL NOTE

NASA TN D-2031

NASA TN D-2031

LOW-SUBSONIC FLIGHT CHARACTERISTICS OF A MODEL OF A SUPERSONIC-AIRPLANE CONFIGURATION WITH A PARAWING AS A LANDING AID

by Joseph L. Johnson, Jr.

Langley Research Center
Langley Station, Hampton, Va.

NATIONAL AERONAUTICS AND SPACE ADMINISTRATION • WASHINGTON, D. C. • NOVEMBER 1963

TECHNICAL NOTE D-2031

LOW-SUBSONIC FLIGHT CHARACTERISTICS OF A MODEL OF A SUPERSONIC-AIRPLANE CONFIGURATION WITH A PARAWING AS A LANDING AID

By Joseph L. Johnson, Jr.

Langley Research Center
Langley Station, Hampton, Va.

NATIONAL AERONAUTICS AND SPACE ADMINISTRATION

LOW-SUBSONIC FLIGHT CHARACTERISTICS OF A MODEL OF A SUPERSONIC-AIRPLANE CONFIGURATION WITH A PARAWING AS A LANDING AID

By Joseph L. Johnson, Jr.

SUMMARY

A wind-tunnel investigation has been conducted at low subsonic speeds to determine the flight characteristics of a model of a supersonic-airplane configuration equipped with a parawing as a landing aid. The model had a 62° delta canard and a 62° delta wing with twin vertical tails located at the 0.27-semispan station. The parawing had a delta planform with a developed area about 60 percent greater than that of the model wing.

The results of the investigation showed that the use of a parawing as a landing and take-off aid appeared to be feasible from the standpoint of stability and control and offered large increases in maximum lift coefficient (which would give substantial reductions in take-off and landing distances) provided the parawing was positioned high enough above the model to prevent large lift losses due to mutual interference effects. The best overall flight behavior was obtained when the tips of the parawing were attached outboard on the model wing to minimize the relative motion between the model and parawing.

INTRODUCTION

The design requirements for efficient supersonic operation of airplanes have resulted in configurations having highly swept, low-aspect-ratio wings which have given rise to some major problem areas in the off-design flight conditions. Research programs are now being conducted by the National Aeronautics and Space Administration which are aimed at solving the off-design problems of supersonic aircraft. In this connection, the results of a recent static force-test investigation (ref. 1) have shown that the use of a parawing which is deployed at low speeds to reduce wing loading appears promising as a take-off and landing aid. The present investigation was conducted to study at low speeds the dynamic stability and control characteristics of a flying model of a supersonic-airplane configuration equipped with a parawing.

The model used in the present investigation was the same as that used in the flight-test investigation reported in reference 2; it had a 62° delta canard and a 62° delta wing with twin vertical tails located at the 0.27-semispan station.

The parawing had a delta planform with a developed area about 60 percent greater than that of the model wing and was attached to the top of the model by several flexible risers. Flight tests were made with the parawing off and with the parawing at several different vertical positions above the model. A motion-picture supplement L-806 covering the flight tests of the model has been prepared and is available on loan. A request card and a description of the film are included at the back of this report.

In addition to the flight tests, force tests were made to determine the static and dynamic stability and control characteristics of the various configurations.

SYMBOLS

All velocities, forces, and moments with the exception of lift and drag were determined with respect to the body axes system originating at the reference center-of-gravity positions shown in figures 1 and 2. The coefficients are based on the dimensional characteristics of the model.

b	wing span, ft
C_A	axial-force coefficient, $F_A/q_\infty S$
C_D	drag coefficient, $F_D/q_\infty S$
C_L	lift coefficient, $F_L/q_\infty S$
C_{L_α}	slope of lift curve
C_l	rolling-moment coefficient, $M_X/q_\infty Sb$
C_m	pitching-moment coefficient, $M_Y/q_\infty S\bar{c}$
C_N	normal-force coefficient, $F_N/q_\infty S$
C_n	yawing-moment coefficient, $M_Z/q_\infty Sb$
C_Y	lateral-force coefficient, $F_Y/q_\infty S$
$\bar{c}$	mean aerodynamic chord, ft
F_A	axial force, lb
F_D	drag, lb
F_L	lift, lb

F_N normal force, lb

F_Y side force, lb

I_X moment of inertia about X-axis, slug-ft^2

I_Y moment of inertia about Y-axis, slug-ft^2

I_Z moment of inertia about Z-axis, slug-ft^2

k reduced frequency parameter, $\omega b/2V$ or $\omega \bar{c}/2V$

L/D lift-drag ratio

M_X rolling moment, ft-lb

M_Y pitching moment, ft-lb

M_Z yawing moment, ft-lb

m mass, slugs

p rolling angular velocity, radians/sec

q pitching angular velocity, radians/sec

q_∞ free-stream dynamic pressure, $\frac{1}{2}\rho V^2$, lb/sq ft

r yawing angular velocity, radians/sec

$\dot{p} = \partial p/\partial t$

$\dot{q} = \partial q/\partial t$

$\dot{r} = \partial r/\partial t$

S wing area, sq ft

t time, sec

V free-stream velocity, ft/sec

X,Y,Z longitudinal, lateral, and normal body axis, respectively

α angle of attack of model center line, deg

$\dot{\alpha}$ rate of change of angle of attack, radians/sec

β angle of sideslip, deg or radians

$\dot{\beta}$ rate of change of sideslip angle, radians/sec

δ_e elevon deflection angle, deg

δ_r rudder deflection angle, deg

μ relative density factor, $m/\rho S\bar{c}$

ρ air density, slugs/cu ft

ϕ angle of roll about X-axis, radians

ψ angle of yaw about Z-axis, radians

ω circular frequency of oscillation, radians/sec

$$C_{N_\alpha} = \frac{\partial C_N}{\partial \alpha} \qquad C_{N_{\dot{\alpha}}} = \frac{\partial C_N}{\partial \frac{\dot{\alpha}\bar{c}}{2V}} \qquad C_{N_q} = \frac{\partial C_N}{\partial \frac{q\bar{c}}{2V}} \qquad C_{N_{\dot{q}}} = \frac{\partial C_N}{\partial \frac{\dot{q}\bar{c}^2}{4V^2}}$$

$$C_{A_\alpha} = \frac{\partial C_A}{\partial \alpha} \qquad C_{A_{\dot{\alpha}}} = \frac{\partial C_A}{\partial \frac{\dot{\alpha}\bar{c}}{2V}} \qquad C_{A_q} = \frac{\partial C_A}{\partial \frac{q\bar{c}}{2V}} \qquad C_{A_{\dot{q}}} = \frac{\partial C_A}{\partial \frac{\dot{q}\bar{c}^2}{4V^2}}$$

$$C_{m_\alpha} = \frac{\partial C_m}{\partial \alpha} \qquad C_{m_{\dot{\alpha}}} = \frac{\partial C_m}{\partial \frac{\dot{\alpha}\bar{c}}{2V}} \qquad C_{m_q} = \frac{\partial C_m}{\partial \frac{q\bar{c}}{2V}} \qquad C_{m_{\dot{q}}} = \frac{\partial C_m}{\partial \frac{\dot{q}\bar{c}^2}{4V^2}}$$

$$C_{l_\beta} = \frac{\partial C_l}{\partial \beta} \qquad C_{l_r} = \frac{\partial C_l}{\partial \frac{rb}{2V}} \qquad C_{l_p} = \frac{\partial C_l}{\partial \frac{pb}{2V}}$$

$$C_{n_\beta} = \frac{\partial C_n}{\partial \beta} \qquad C_{n_r} = \frac{\partial C_n}{\partial \frac{rb}{2V}} \qquad C_{n_p} = \frac{\partial C_n}{\partial \frac{pb}{2V}}$$

$$C_{Y_\beta} = \frac{\partial C_Y}{\partial \beta} \qquad C_{Y_r} = \frac{\partial C_Y}{\partial \frac{rb}{2V}} \qquad C_{Y_p} = \frac{\partial C_Y}{\partial \frac{pb}{2V}}$$

$$C_{l_{\dot{\beta}}} = \frac{\partial C_l}{\partial \frac{\dot{\beta}b}{2V}} \qquad C_{l_{\dot{r}}} = \frac{\partial C_l}{\partial \frac{\dot{r}b^2}{4V^2}} \qquad C_{l_{\dot{p}}} = \frac{\partial C_l}{\partial \frac{\dot{p}b^2}{4V^2}}$$

$$C_{n_{\dot{\beta}}} = \frac{\partial C_n}{\partial \frac{\dot{\beta} b}{2V}} \qquad C_{n_{\dot{r}}} = \frac{\partial C_n}{\partial \frac{\dot{r} b^2}{4V^2}} \qquad C_{n_{\dot{p}}} = \frac{\partial C_n}{\partial \frac{\dot{p} b^2}{4V^2}}$$

$$C_{Y_{\dot{\beta}}} = \frac{\partial C_Y}{\partial \frac{\dot{\beta} b}{2V}} \qquad C_{Y_{\dot{r}}} = \frac{\partial C_Y}{\partial \frac{\dot{r} b^2}{4V^2}} \qquad C_{Y_{\dot{p}}} = \frac{\partial C_Y}{\partial \frac{\dot{p} b^2}{4V^2}}$$

The term "in-phase derivative" used herein refers to any one of the stability derivatives which are based on the forces or moments in phase with the angle of attack, roll, yaw, or sideslip produced in the oscillatory tests. The term "out-of-phase derivative" refers to any one of the stability derivatives which are based on the forces or moments 90° out of phase with the angle of attack, roll, yaw, or sideslip. The derivatives were measured in the oscillation tests in the following combinations:

In-phase pitching derivatives:

$$C_{N_\alpha} - k^2 C_{N_{\dot{q}}}$$

$$C_{A_\alpha} - k^2 C_{A_{\dot{q}}}$$

$$C_{m_\alpha} - k^2 C_{m_{\dot{q}}}$$

In-phase rolling derivatives:

$$C_{l_\beta} \sin \alpha - k^2 C_{l_{\dot{p}}}$$

$$C_{n_\beta} \sin \alpha - k^2 C_{n_{\dot{p}}}$$

$$C_{Y_\beta} \sin \alpha - k^2 C_{Y_{\dot{p}}}$$

In-phase yawing derivatives:

$$C_{l_\beta} \cos \alpha + k^2 C_{l_{\dot{r}}}$$

$$C_{n_\beta} \cos \alpha + k^2 C_{n_{\dot{r}}}$$

$$C_{Y_\beta} \cos \alpha + k^2 C_{Y_{\dot{r}}}$$

Out-of-phase pitching derivatives:

$$C_{m_q} + C_{m_{\dot{\alpha}}}$$

$$C_{A_q} + C_{A_{\dot{\alpha}}}$$

$$C_{N_q} + C_{N_{\dot{\alpha}}}$$

Out-of-phase rolling derivatives:

$$C_{l_p} + C_{l_{\dot{\beta}}} \sin \alpha$$

$$C_{n_p} + C_{n_{\dot{\beta}}} \sin \alpha$$

$$C_{Y_p} + C_{Y_{\dot{\beta}}} \sin \alpha$$

Out-of-phase yawing derivatives:

$$C_{l_r} - C_{l_{\dot{\beta}}} \cos \alpha$$

$$C_{n_r} - C_{n_{\dot{\beta}}} \cos \alpha$$

$$C_{Y_r} - C_{Y_{\dot{\beta}}} \cos \alpha$$

APPARATUS AND TESTING TECHNIQUE

Model

The model used in the investigation was the same as that employed in the flight-test investigation reported in reference 2. This model had an elliptical-cross-section fuselage with major axis horizontal, a 62° delta canard surface, and a 62° delta wing with twin vertical tails located at the 0.27-semispan station. A three-view drawing of the model is presented in figure 2. As illustrated in the figure, the basic elevons on the model were provided with a spanwise extension. This extension could be linked to the basic surfaces for increased control if desired.

The parawing used on the model was the same as that utilized in the force-test investigation of reference 1. The parawing had a developed sweep of 45° and an area 60 percent greater than that of the model wing. The leading edges and keel consisted of three aluminum tubes (0.0125 keel length in diameter) of equal length which were connected at the nose of the parawing by three flat springs. With this construction either an up or down deflection of the parawing nose could

be obtained, depending on the initial setting of the springs. The fabric used to form the membrane of the parawing consisted of nylon rip-stop parachute cloth. The cloth was plastic coated to give essentially zero porosity.

The parawing was attached to the model by six 1/32-inch steel cables or risers. The lengths of these cables and also the rigging used to attach the parawing to the model were varied during the tests. The attachment points, riggings, and parawing vertical locations used during the tests are illustrated in figures 3(a) and 3(b). The four test arrangements included the parawing in position 1 (same parawing location, attachment points, and rigging as those used in the force-test studies of ref. 1), position 2 (parawing tip risers moved from fuselage attachment points to wing tip while parawing vertical location remained unchanged), position 3 (rigging the same as that for position 2 but height of parawing reduced by one-half), and position 4 (rigging the same as the rigging for positions 2 and 3 but height of parawing reduced to zero). The height was taken as the distance of the aft end of the keel above the model. It should be pointed out that, as the parawing was lowered, it also moved forward with respect to the model. The parawing had approximately a 30° angle with respect to the model center line for all conditions.

The dimensional and mass characteristics of the basic model and parawing are listed in table I and the riser lengths used in the investigation are presented in table II.

Test Equipment

Static and dynamic force tests were conducted in a low-speed wind tunnel having a 12-foot octagonal test section at the Langley Research Center. These tests were made of the flight-test configurations by using a sting-type support system and strain-gage balances. A description of the force-test equipment is given in reference 3.

The flight tests were made in the Langley full-scale tunnel. A sketch of the test setup is presented in figure 4 and photographs of the model flying in the tunnel are shown as figure 5. A complete description of the flight-test equipment and setup is given in reference 4.

TESTS

Flight Tests

Flight tests were made to determine the dynamic stability and control characteristics and general flight behavior of the model with a parawing installed at several different vertical locations and with several variations in the rigging. A few flights were also made of the model alone for comparison purposes. Most of the flights to determine the effects of parawing location were made at approximately constant angles of attack from about 17° to 20°. No flights were attempted at higher angles of attack but a few flights were made at an angle of attack as

low as 13°. The flight tests were made over a speed range from about 38 feet per second to 55 feet per second. This speed range corresponds to a dynamic-pressure range from 1.67 pounds per square foot to 5.5 pounds per square foot and to a Reynolds number range from about 0.70×10^6 to 1.01×10^6 based on the mean aerodynamic chord of the wing.

The center of gravity used in the flight tests was located at the 0.10 mean aerodynamic chord of the basic model. In all flights, the canard surface was fixed at 0° incidence and longitudinal trim and control were achieved through symmetrical deflection of the elevons. Lateral control was obtained through coordination of rudder deflection with differential deflection of the elevons. Flicker-type controls (full on and off) were used in these tests, and the control deflections were ±10° for elevator control, ±10° for rudder control, and ±12° for aileron control. A few flights were made with the basic elevon surfaces but most of the flights of the model-parawing combination were made with the elevon surfaces increased by extending the span (see fig. 2).

Thrust for the flight tests was obtained from an air nozzle which was located in the engine pack and was supplied with compressed air through a flexible hose. The hose was attached to the model at about the center-of-gravity location.

The model behavior during flight was observed by the pitch pilot located at the side of the test section and by the roll-yaw pilot located at the rear of the test section. The results obtained in the flight tests were primarily in the form of qualitative ratings of flight behavior based on pilot opinion. Motion-picture records obtained in the tests were used to verify and correlate the ratings for the different flight conditions. These motion-picture records were obtained with cameras located at the side of the test section and at the top and bottom of the exit cone.

Force Tests

Force tests were made over an angle-of-attack range from -3° to 30° to determine the static longitudinal and lateral stability and control characteristics and the oscillatory stability derivatives of the flight-test configurations for correlation with flight-test results. The configurations tested included the model alone and the model with the parawing in positions 1 to 4. In addition, force tests were made to determine the static stability characteristics of the model with the parawing mounted in position but not attached to the model. In this way interference effects of the parawing on the model could be determined.

The static lateral stability characteristics were measured over an angle-of-sideslip range from -20° to 20°. The rotary oscillation tests were made in roll, yaw, and pitch for amplitudes of ±5°. Most of the oscillation tests were made for a frequency of 0.5 cycle per second which corresponds to a reduced-frequency parameter of 0.10 in the longitudinal tests and of 0.167 in the lateral tests.

Most of the tests were made at a dynamic pressure of 2.54 pounds per square foot which corresponds to an airspeed of about 46 feet per second. Some of the tests were made at a dynamic pressure of 1.67 pounds per square foot which

corresponds to an airspeed of about 38 feet per second. The Reynolds number of the tests varied from about 0.70×10^6 to 0.865×10^6 based on the mean aerodynamic chord of the model wing.

STATIC STABILITY AND CONTROL CHARACTERISTICS OF THE FLIGHT-TEST MODEL

Static Longitudinal Stability and Control

The effect of the parawing on the static longitudinal stability characteristics of the model is shown in figures 6(a) to 6(d) for parawing positions 1 to 4, respectively. A summary of the results is given in figure 6(e). The data show that the model alone was stable up to 15° but very unstable at higher angles of attack. Generally similar trends were obtained for the combination with the parawing in position 1, 2, or 3 although there was some change in the degree of stability or instability in these configurations. With the parawing in position 4, the combination showed instability above about 10° angle of attack and a large positive shift in the pitching-moment curve over the angle-of-attack range. The addition of the parawing added an increment of lift and drag to the model at a given angle of attack for all positions tested. As expected, the lift increments were greatest for positions 1 and 2 (highest position tested) and decreased as the parawing was lowered. For all configurations tested the maximum lift-drag ratio was greatly reduced by the addition of the parawing.

In an effort to obtain some information for use in interpreting the results of figure 6, the lift, drag, and pitching-moment characteristics of the model were measured with the parawing mounted in position 1, 2, 3, or 4 but not attached by risers to the model. The results of these tests, which are presented in figure 7(a), show that the parawing reduced the lift-curve slope and delayed the stall of the model to a higher angle of attack. These effects are probably related to a large extent to the influence of the downwash from the parawing on the flow characteristics of the model. The results of figure 7(a) are in agreement with those of earlier work with biplanes (for example, ref. 5) in which it was found that the upper wing influenced the lift characteristics of the lower wing in much the same manner. The pitching-moment data of figure 7(a) show that the parawing reduced the stability of the model at the lower angles of attack and also reduced the instability at higher angles of attack, resulting in more nearly linear pitching-moment curves.

In order to obtain some indication of the direct contribution of the parawing to the combination, the data of figure 7(a) were subtracted from the data of figure 6(e); the results are presented in figure 7(b). From the incremental longitudinal characteristics presented in this figure, it is seen that the parawing in positions 1, 2, and 3 was stabilizing up to about 15° angle of attack and then was generally destabilizing at the higher angles of attack. In position 4, the parawing was destabilizing over the test angle-of-attack range.

Static Lateral Stability and Control

The static lateral stability coefficients are presented in figure 8(a) for model alone and in figures 8(b) to 8(e) for parawing positions 1 to 4, respectively. These data are generally linear for small sideslip angles except for the yawing-moment coefficients for some conditions at high angles of attack. The lateral stability parameters C_{Y_β}, C_{n_β}, and C_{l_β} determined for angles of sideslip of $\pm 5^\circ$ from figure 8 are presented as a function of angle of attack and lift coefficient in figure 9.

The data of figure 9 show that, for a given angle of attack, adding the parawing generally resulted in higher values of $-C_{Y_\beta}$, C_{n_β}, and $-C_{l_\beta}$ than for the model alone. It is seen that the parawing did not have a large effect on $-C_{l_\beta}$ in the low lift-coefficient range but did extend the linear range of $-C_{l_\beta}$ to much higher lift coefficients (bottom right-hand plot).

In order to determine the induced effects of the parawing on the lateral stability characteristics of the model, tests were made in which C_{Y_β}, C_{n_β}, and C_{l_β} were determined for the model with the parawing mounted in position but not attached to the model. The results of these tests are compared with results for the model alone in figure 10 and show that the only major effect of the parawing was on $-C_{l_\beta}$. These data indicate (with the exception of those for position 4) that the linear range of $-C_{l_\beta}$ was extended to a higher angle of attack. This induced effect, which is reflected in the data for the combination, is probably an indication of a delay in wing stall.

The static lateral control characteristics of the model are presented in figures 11(a) to 11(c). The data of figure 11(a) show that the addition of the parawing caused some reduction in the rolling effectiveness of the ailerons except at high angles of attack. The parawing had no appreciable effect on the yawing moment produced by aileron deflection except in position 2 where the angle of attack at which the yawing moment became adverse was decreased from 29° to 17°.

Presented in figure 11(b) is a comparison of the aileron effectiveness for the basic control surfaces (used in the flight-test investigation reported in reference 2 and in a few tests of the present investigation) with that for the large control surfaces with the parawing in position 2. The data show that the large surfaces had about double the rolling effectiveness of the basic surfaces but generally had no appreciable effect on the yawing moment produced by aileron deflection.

The rudder-effectiveness data presented in figure 11(c) show that, in general, the addition of the parawing decreased the yawing moment produced by rudder deflection over the test angle-of-attack range.

Longitudinal Oscillatory Derivatives

In-phase derivatives.- The longitudinal derivatives obtained in phase with angular displacement during pitching-oscillation tests of the model are presented in figures 12(a) to 12(c). Also presented in these figures for the purpose of comparison are static values (k = 0) of the longitudinal stability parameters taken from figure 6(e). These data show that the static and oscillatory results are generally in good agreement as far as the trends of the data are concerned, although there are some differences in the values of the derivatives. Static data for the canard-off configuration are not presented since this configuration was not tested in the static force tests.

Out-of-phase derivatives.- The longitudinal derivatives measured out of phase with angular displacement in the pitching-oscillation tests are presented as functions of angle-of-attack and lift coefficient in figure 13. The data show that the basic model had positive damping in pitch (negative values of $C_{m_q} + C_{m_{\dot{\alpha}}}$) that increased up to an angle of attack of about 20° and then decreased slightly. The data also show that the parawing did not greatly affect the damping for a given angle of attack.

In comparing the angle-of-attack results of figure 13, it is important to remember the relative difference in lift coefficient for the model alone and the model-parawing combination. For this reason, the data are replotted against lift coefficient on the right-hand side of figure 13. When the higher lift coefficients for the model-parawing combination are taken into account, it is evident that for a given lift coefficient the damping of the model was generally reduced by the addition of the parawing This result is probably related mainly to the difference in flow-separation effects for the two configurations. For instance, the longitudinal data of figure 7 show that the parawing reduced the lift-curve slope and delayed the angle of stall of the model (which indicates that flow-separation effects were delayed). It is likely, therefore, that the $C_{m_{\dot{\alpha}}}$ component of the total derivative, which is a function of flow separation, was reduced by the addition of the parawing.

Lateral Oscillatory Derivatives

In-phase derivatives.- The lateral derivatives obtained in phase with angular displacement during the rolling and yawing oscillation tests are presented in figure 14. Also presented in this figure for purposes of comparison are static values (k = 0) of the lateral stability parameters taken from figure 9. In general, the static and oscillatory test results show similar trends with angle of attack although there are some fairly large differences in the magnitude of the two sets of data for some conditions.

Out-of-phase derivatives.- Values of the out-of-phase derivatives measured in the rolling and yawing oscillation tests are presented in figure 15(a) and figure 15(b), respectively. The data show that the damping-in-roll parameter $C_{l_p} + C_{l_{\dot{\beta}}} \sin \alpha$ of the model alone became more negative (increased damping) as the angle of attack increased. The addition of the parawing resulted in an

increase in damping in the low angle-of-attack range and a decrease in damping in the high angle-of-attack range. The yawing oscillation data of figure 15(b) show that the parawing position had no large or systematic effect on the damping-in-yaw parameter $C_{n_r} - C_{n_{\dot{\beta}}} \cos \alpha$ or the rolling-moment parameter $C_{l_r} - C_{l_{\dot{\beta}}} \cos \alpha$ except in the high angle-of-attack range where the parawing caused a large reduction in the rolling-moment-parameter values.

These effects at high angles of attack, brought about by the addition of the parawing, are believed to be associated primarily with the reduction in the $C_{l_{\dot{\beta}}}$ derivative of the model wing caused by a delay in flow separation on the wing in the presence of the parawing. The results of reference 6 substantiate this reasoning, give a more thorough explanation of the effects of flow separation, and establish relationships which correlate these effects with the static and oscillatory lateral stability derivatives.

FLIGHT-TEST RESULTS AND DISCUSSION

Most of the flight tests to evaluate the effect of the parawing on the flight characteristics of the model were made for approximately constant angle-of-attack conditions ($\alpha = 17^\circ$ to 20°). Since the addition of the parawing usually provided a substantial increase in lift coefficient, the trim speed in the test angle-of-attack range was generally considerably lower for the model-parawing combination than for the model alone. With a differential elevon deflection of $\pm 12^\circ$ for aileron control, it was found that the control effectiveness provided by the basic surfaces was adequate for flying the combination under relatively undisturbed conditions, but most of the flights of the combination were made with the larger elevons to provide increased control effectiveness at the lower trim speeds. The larger elevons gave too much control effectiveness at the higher speeds flown for the model alone.

Because of the increase in the ratio of moments of inertia to aerodynamic damping moments and the reduction in control effectiveness as the trim speed was reduced, the model angular motions after given control deflections were much slower for the model-parawing combination than for the model alone. This effect, in addition to the decrease in gust intensity of the tunnel at the lower speeds, resulted in an increase in flight steadiness and ease of flying which generally led to better overall flight behavior for the model-parawing combination than for the model alone.

Longitudinal Stability and Control

Flight characteristics of the model alone were generally similar to those reported in reference 2 - that is, the model had satisfactory dynamic behavior at the lower angles of attack but had unsatisfactory flight characteristics at the higher angles of attack because of static longitudinal instability. This instability resulted in a tendency of the model to diverge in pitch and required careful attention to controls to keep the model flying.

The flight characteristics of the model with the parawing in positions 1, 2, and 3 were found to be satisfactory over the test angle-of-attack range and were considerably better than those for the model alone. The static longitudinal instability indicated for these configurations near 20° angle of attack (see fig. 6(e)) did not appear to be a problem as it had been for the model alone. (The reasons for this difference in dynamic behavior are discussed subsequently.) The control characteristics were considered to be good. Relatively smooth flights could be made with little attention to controls, and recovery from disturbances was generally easily accomplished. The best longitudinal flight behavior was obtained with the parawing in positions 2 and 3 where the risers from the tips of the parawing were attached outboard on the wing of the model. This arrangement kept the relative motion between the parawing and the model to a minimum and resulted in somewhat steadier flights than those with the risers attached inboard (position 1). With the parawing rigged in position 1, the leading edges moved in and out as the model pitched which resulted in a constantly changing angle of sweep. This effect was not too objectionable from the standpoint of overall flight behavior but probably accounted for some of the unsteadiness experienced with this arrangement.

Lowering the height of the parawing from position 2 to position 3 did not greatly affect the dynamic behavior of the model. When the parawing was lowered to position 4, however, it was found that the model did not fly as smoothly as it did when the parawing was higher. This condition appears to be of little practical importance because of the loss in lift when the parawing is in close proximity to the model. The general flight behavior was believed to deteriorate considerably in changing to this parawing position but the model was flyable (despite the apparent high degree of static longitudinal instability indicated by the force-test results of fig. 6(e)), although considerably more attention to the control was required.

One interesting point brought out in the flight tests was that the static longitudinal instability of the parawing-model combination did not appear to adversely affect the dynamic longitudinal behavior as much as it did for the model alone even though the static pitching-moment characteristics C_{m_α} did not appear to be appreciably different for the two configurations (fig. 6(e)). It was first assumed that this beneficial effect of the parawing was probably a result of increased damping in pitch but oscillation tests indicated that the damping in pitch for the combination was not greatly different from that of the model alone. It was therefore necessary to examine other longitudinal parameters in an effort to determine which parameters were mainly responsible for the flight behavior for this arrangement.

From past experience in flying statically unstable models, it has been shown that the most rearward center-of-gravity location where sustained flights were possible corresponded to that of the stick-fixed maneuver point (for example, see ref. 4). An analysis of two-degree-of-freedom longitudinal stability equations indicates that the value of C_{m_α} corresponding to this center-of-gravity location can be defined as $\frac{-(C_{L_\alpha})\,(C_{m_q} + C_{m_{\dot{\alpha}}})}{4\mu}$. This expression shows that the maneuver point varies directly with C_{L_α} and $C_{m_q} + C_{m_{\dot{\alpha}}}$. In the investigation of

reference 4 it was shown experimentally that the maneuver point could be shifted rearward a considerable amount by the addition of artificial damping in pitch. In the investigation of reference 7 where an automatic control system was used to vary C_{m_α} and C_{L_α} it was found that a small amount of static longitudinal instability could be tolerated provided it was accompanied by an increase in C_{L_α}.

In order to determine the stick-fixed maneuver-point boundary for each of the configurations investigated, calculations were made by using measured aerodynamic data and the results are presented in figure 16. Also presented in these plots are the values of $C_{m_q} + C_{m_{\dot{\alpha}}}$ and C_{m_α} corresponding to the flight-test conditions. These results show that the flight-test point for the model alone was in the region of negative maneuver margin where past experience has shown that models were either unflyable or very difficult to fly. On the other hand, most of the flight-test points for the model-parawing combination were in the region of positive maneuver margin where past experience has shown that statically unstable models could be flown satisfactorily. From these results, it appears that the increased lift-curve slope and slight reductions in static longitudinal instability were significant factors involved in the favorable effect of the parawing on the dynamic longitudinal behavior of the model at high angles of attack.

Lateral Stability and Control

In order to obtain some indication of the relative difference in the response characteristics of the model alone and model-parawing combination for use in the discussion of the lateral flight-test results, calculations were made (on the assumption that the model had only freedom in roll) for the various configurations tested and the results are presented in figure 17. Since the static aileron control data indicated no major effect of the parawing on the aileron control characteristics, the calculations were made for a constant value of ΔC_l in order to show the relative effects of the aerodynamic and inertia factors for the configurations involved. The relative differences in roll rates shown by the results of figure 17 are believed to be valid representations of those experienced in the flight tests and can be attributed, to a large extent, to the differences in trim speeds for the various test conditions. These results indicate that with the parawing in either position 1 or position 2 the roll rate was about one-third of that for the model alone. As the parawing was lowered, the roll rate of the combination increased and was about two-thirds of that of the model alone for the combination with the parawing in position 4.

Model alone.- The dynamic lateral stability and control characteristics of the model alone were similar to those reported in reference 2. The Dutch roll oscillation was fairly well damped and the model could be flown fairly smoothly by giving careful attention to the control.

Model with parawing in position 1.- The parawing in position 1 had considerable freedom of movement with respect to the model. This condition was annoying to the pilot and made the model difficult to fly smoothly. It was found that the model would respond to a control input but the parawing would lag behind; this condition resulted in the model and parawing being out of phase. This condition

would also occur due to gust disturbances. This out-of-phase motion made steady flying difficult because the model or parawing always appeared to be moving, but there was no particular difficulty in maintaining flight in any desired part of the test section despite the reduction in roll rate indicated by the data of figure 17. The Dutch roll oscillation appeared to be well damped and the general flight behavior was considered to be better than that for the model alone, probably mainly because of the increase in flight steadiness resulting from the slower motions associated with the lower trim speeds at which the model was flying.

Model with parawing in position 2.- Flight tests with the parawing in position 2 showed that there was very little of the relative motion between the model and parawing noted for position 1; the model and parawing appeared to roll and yaw together. Consequently, the model was much easier to fly, and smooth sustained flights could be made with very little effort on the part of the pilot. The Dutch roll damping appeared to be about the same for either parawing position 1 or 2, but because of the improvement in flight steadiness the general flight behavior for position 2 was better than that for position 1.

With the parawing in position 2, the model was flown at an angle of attack as low as 13° in an effort to study the effect of higher speed on the characteristics of this configuration. The flights were not as smooth and appeared to have some of the erratic behavior noted for the model alone; this condition probably stemmed from the increase in gust intensity and control effectiveness associated with the higher speed.

A few tests were made in which ailerons-alone control was compared with coordinated aileron and rudder control. The results of these tests indicated that the model could be flown about as easily with ailerons alone as with the ailerons and rudders although there was more yawing motion evident with ailerons alone and the rudders made recovery from large disturbances somewhat easier. These tests were made at about 18° angle of attack where the aileron yawing moments were about zero (see fig. 11(a)). If the tests had been made at a higher angle of attack where the yawing moments were adverse, flights with ailerons alone might not have been possible. In a few tests in which this arrangement was flown with the basic elevons it was found that the decreased control effectiveness (roll effectiveness reduced by a factor of two, fig. 11(b)) was still adequate for flying the model under relatively undisturbed conditions, but it was much more difficult to position the model in the tunnel and to recover from large disturbances.

Model with parawing in position 3.- With the parawing height reduced to one-half that of positions 1 and 2 it was found that the stability and control and general flight behavior were essentially the same as those with the parawing in position 2. There was very little relative motion between the parawing and model, and smooth sustained flights were possible with very little effort on the part of the pilot.

Model with parawing in position 4.- With the parawing height reduced to zero (position 4), the model motions were about as erratic as those of the model alone. Also, the Dutch roll oscillation for this parawing position was not as heavily damped and the lateral control appeared to be somewhat weaker than those for the other parawing positions despite the fact that most of the flights were made at

higher speeds. In general, it appeared that this configuration was more easily disturbed and more difficult to recover than the other parawing configurations investigated.

The decrease in control effectiveness noted for position 4 appears to contradict the static force-test results of figure 11 which showed about the same general aileron and rudder effectiveness for all parawing positions. The reason for the decrease in effectiveness noted in the flight tests is not known but it might be caused by some interference effect from the parawing which introduced large changes in the static or dynamic stability derivatives whenever the model rolled or yawed.

CONCLUDING REMARKS

The results of the investigation indicated that the use of a parawing as a landing and take-off aid appeared to be feasible from the standpoint of stability and control and offered large increases in maximum lift coefficient (which would give substantial reductions in take-off and landing distances) provided the parawing was positioned high enough above the model to prevent large lift losses due to mutual interference effects. The best overall flight behavior was obtained when the tips of the parawing were attached outboard on the wing to minimize relative motion between the model and parawing.

Langley Research Center,
National Aeronautics and Space Administration,
Langley Station, Hampton, Va., August 23, 1963.

REFERENCES

1. Naeseth, Rodger L.: An Exploratory Study of a Parawing as a High-Lift Device for Aircraft. NASA TN D-629, 1960.

2. Johnson, Joseph L., Jr.: Wind-Tunnel Investigation of Low-Subsonic Flight Characteristics of a Model of a Canard Airplane Designed for Supersonic Cruise Flight. NASA TM X-229, 1960.

3. Hewes, Donald E.: Low-Subsonic Measurements of the Static and Oscillatory Lateral Stability Derivatives of a Sweptback-Wing Airplane Configuration at Angles of Attack From -10° to 90°. NASA MEMO 5-20-59L, 1959.

4. Paulson, John W., and Shanks, Robert E.: Investigation of Low-Subsonic Flight Characteristics of a Model of a Hypersonic Boost-Glide Configuration Having a 78° Delta Wing. NASA TN D-894, 1961. (Supersedes NASA TM X-201.)

5. Fairbanks, A. J.: Pressure Distribution Tests on PW-9 Wing Models Showing Effects of Biplane Interference. NACA Rep. 271, 1927.

6. Campbell, John P., Johnson, Joseph L., Jr., and Hewes, Donald E.: Low-Speed Study of the Effect of Frequency on the Stability Derivatives of Wings Oscillating in Yaw With Particular Reference to High Angle-of-Attack Conditions. NACA RM L55H05, 1955.

7. Brissenden, Roy F., Alford, William L., and Mallick, Donald L.: Flight Investigation of Pilot's Ability to Control an Airplane Having Positive and Negative Static Longitudinal Stability Coupled With Various Effective Lift-Curve Slopes. NASA TN D-211, 1960.

TABLE I.- DIMENSIONAL AND MASS CHARACTERISTICS OF BASIC MODEL AND PARAWING

Weight of basic model, lb	31
Wing loading, lb/sq ft	2.86
Moment of inertia, slug-ft^2:	
I_X	0.43
I_Y	4.10
I_Z	4.90
Wing:	
Area, sq ft	10.86
Span, ft	4.87
Aspect ratio	2.19
Mean aerodynamic chord, ft	2.93
Root chord, ft	4.38
Tip chord, ft	0
Sweep of leading edge, deg	62
Airfoil section	Triangular, flat lower surface
Airfoil thickness (maximum thickness at 70-percent-chord line), percent chord	2.5
Vertical tail:	
Area (each, to ref. line), sq ft	0.78
Span, ft	0.863
Aspect ratio	0.954
Root chord, ft	1.33
Tip chord, ft	0.41
Sweep of leading edge, deg	52
Airfoil section	Double wedge
Airfoil thickness (maximum thickness at 70-percent-chord line), percent chord	2.5
Canard surface:	
Area (includes area covered by fuselage), sq ft	1.49
Span, ft	1.78
Aspect ratio	2.13
Sweep of leading edge, deg	62
Airfoil section	Double wedge
Airfoil thickness (maximum thickness at 70-percent-chord line), percent chord	2.5
Elevon, basic:	
Area (each), sq ft	0.29
Span, ft	0.765
Chord, ft	0.406
Elevon, large:	
Area (each), sq ft	0.490
Span, ft	1.26
Chord, ft	0.406
Parawing:	
Weight, lb	2.7
Area (developed, 45° leading-edge sweep), sq ft	17
Span, ft	7.28
Root chord, ft	5.00

TABLE II.- RISER LENGTHS USED IN THE TESTS

Wing position	Riser (see fig. 3)	Riser length, in.
1	a	35.25
	b	35.50
	c	35.25
	d	44.25
	e	18.75
	f	44.25
2	a	35.25
	b	35.50
	c	35.25
	d	20.75
	e	18.75
	f	20.75
3	a	26.0
	b	26.50
	c	26.0
	d	10.50
	e	9.38
	f	10.50
4	a	17.25
	b	17.50
	c	17.25
	d	2.75
	e	0
	f	2.75

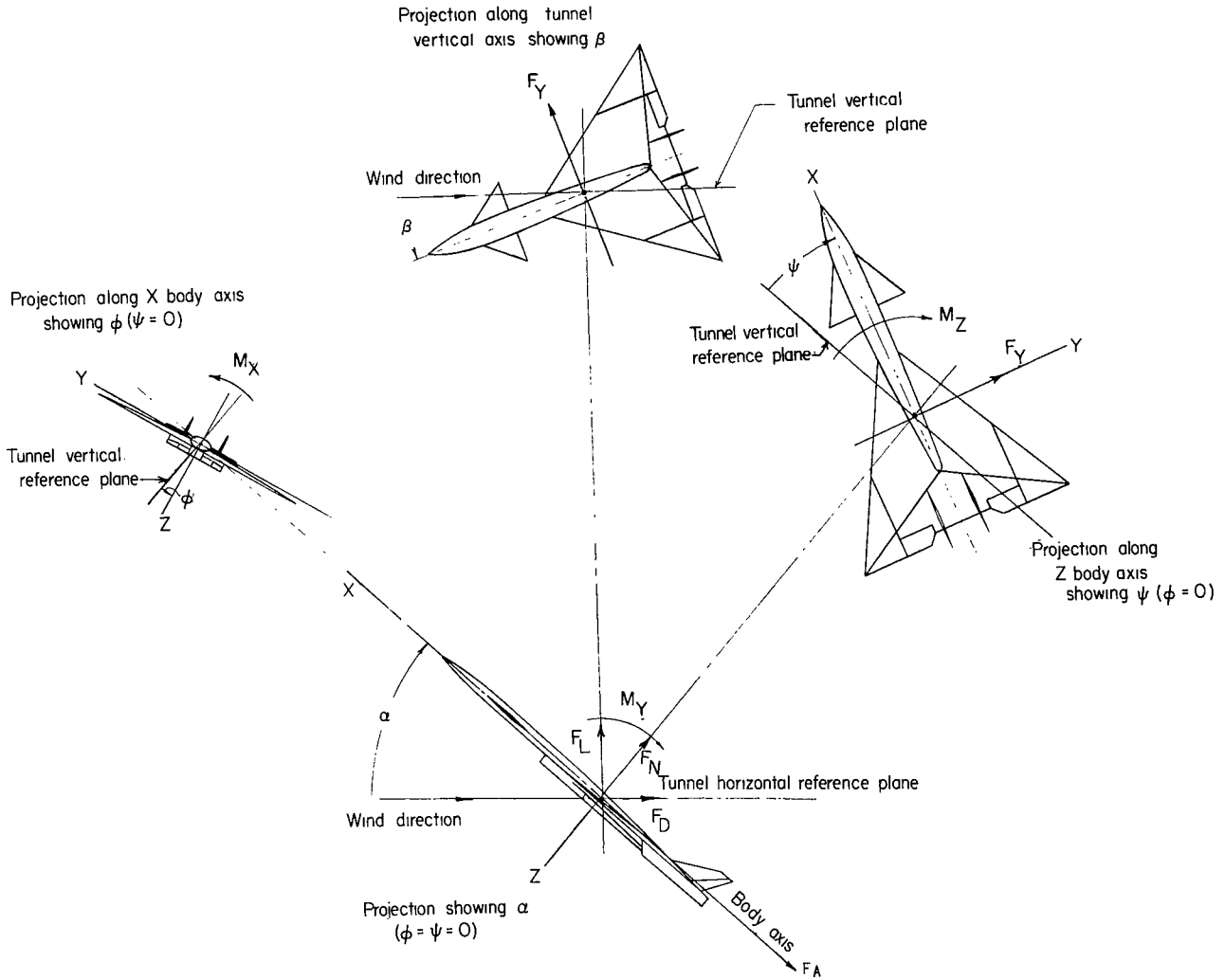

Figure 1.- The body system of axes. Arrows indicate positive directions of moments, forces, and angles. This system of axes is defined as an orthogonal system having the origin at the center of gravity and in which the X-axis is in the plane of symmetry and alined with the longitudinal axis of the fuselage, the Z-axis is in the plane of symmetry and perpendicular to the X-axis, and the Y-axis is perpendicular to the plane of symmetry.

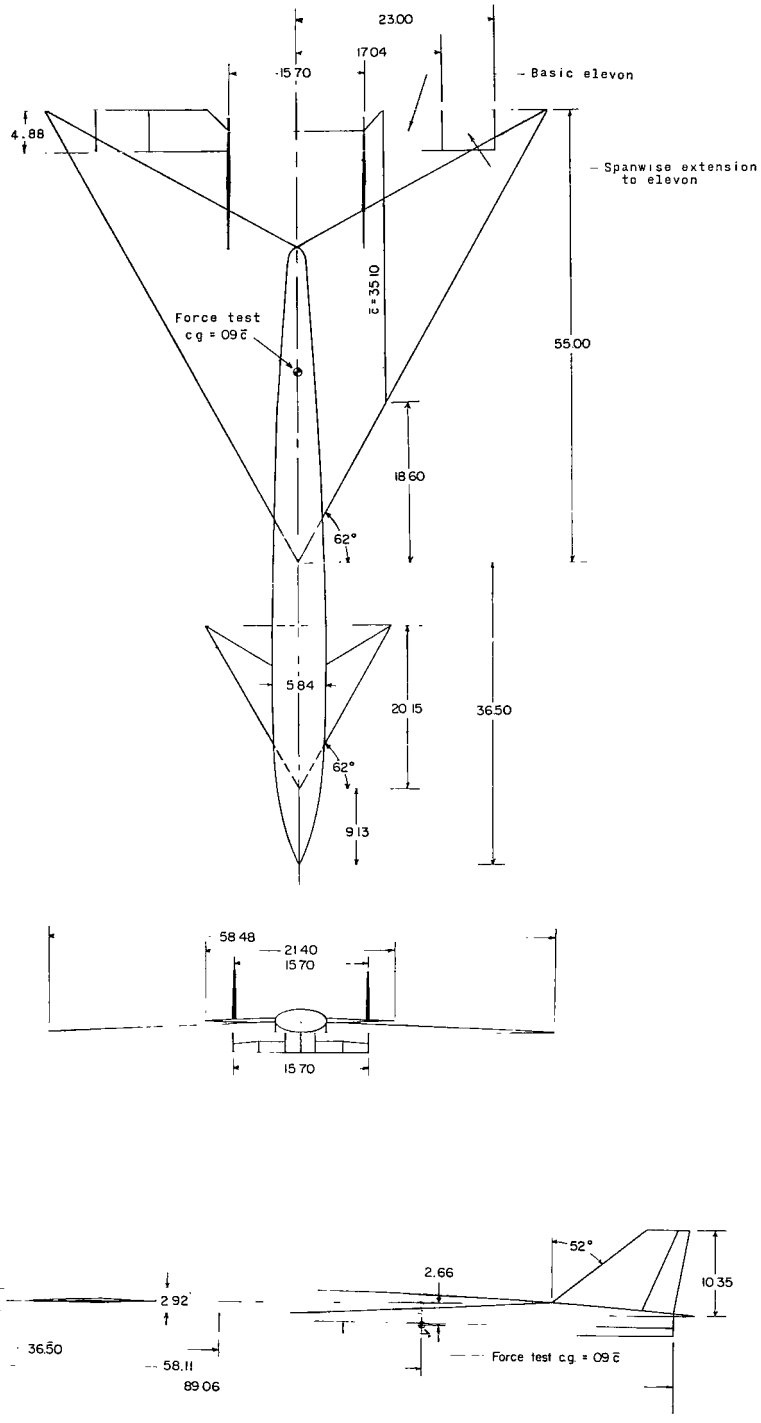

Figure 2.- Dimensional characteristics of the model used in the investigation. All dimensions are in inches unless otherwise indicated.

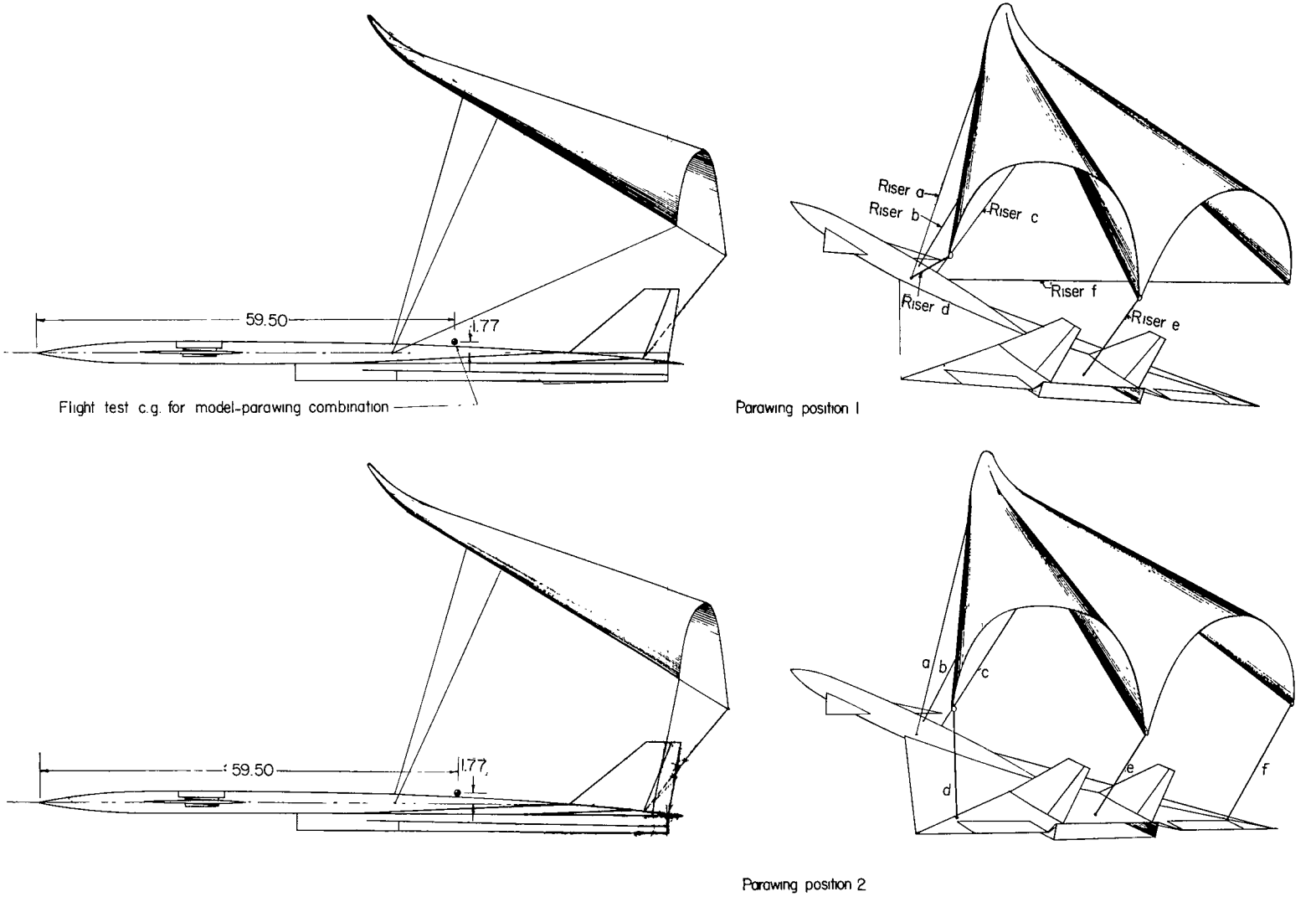

(a) Parawing positions.

Figure 3.- Sketches of model-parawing combinations used in the investigation. All dimensions are in inches unless otherwise indicated. (See table II for riser dimensions.)

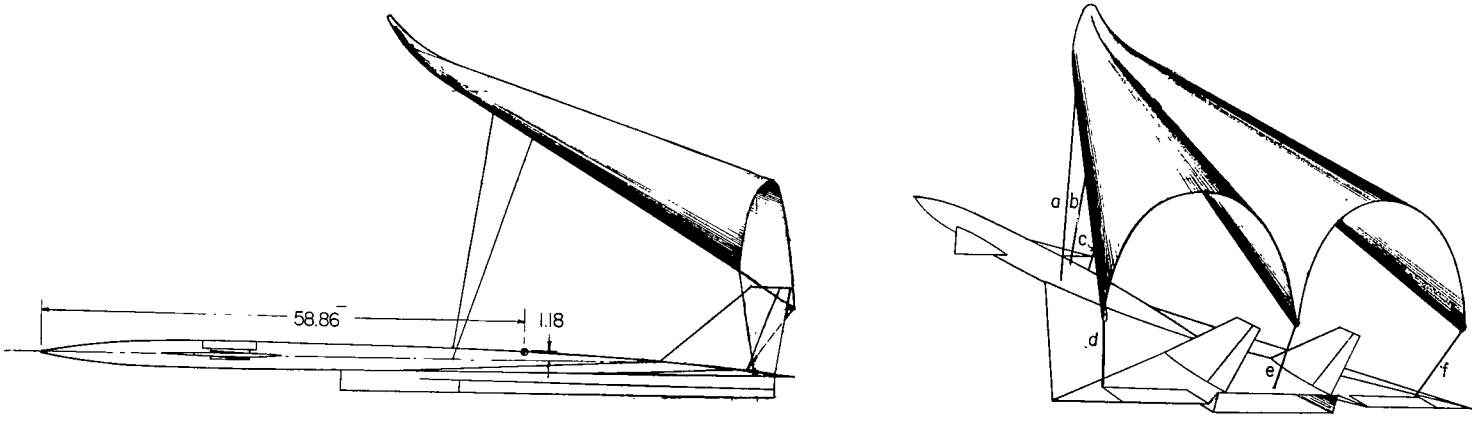

Parawing position 3

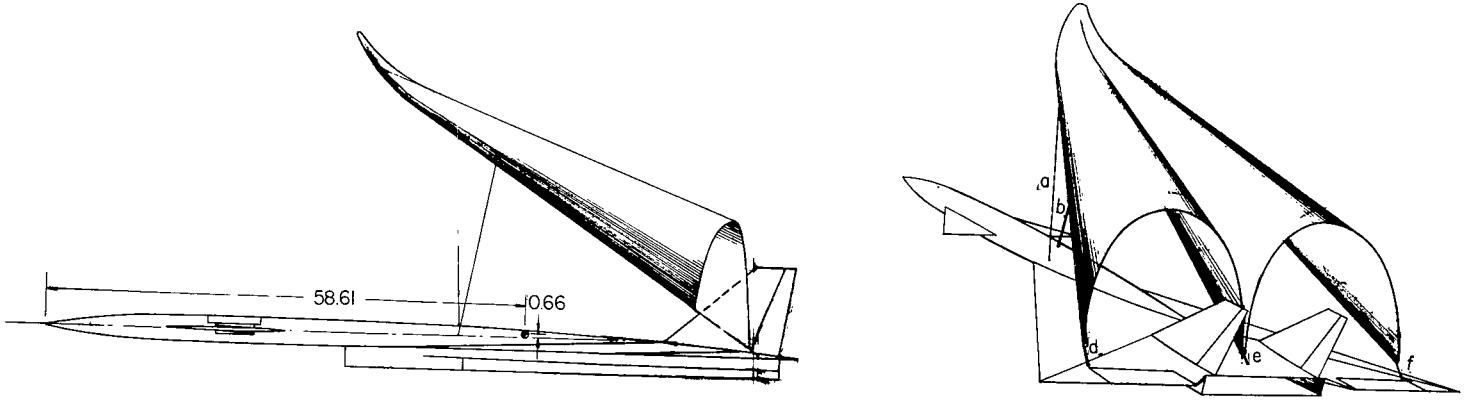

Parawing position 4

(a) Concluded.

Figure 3.- Continued.

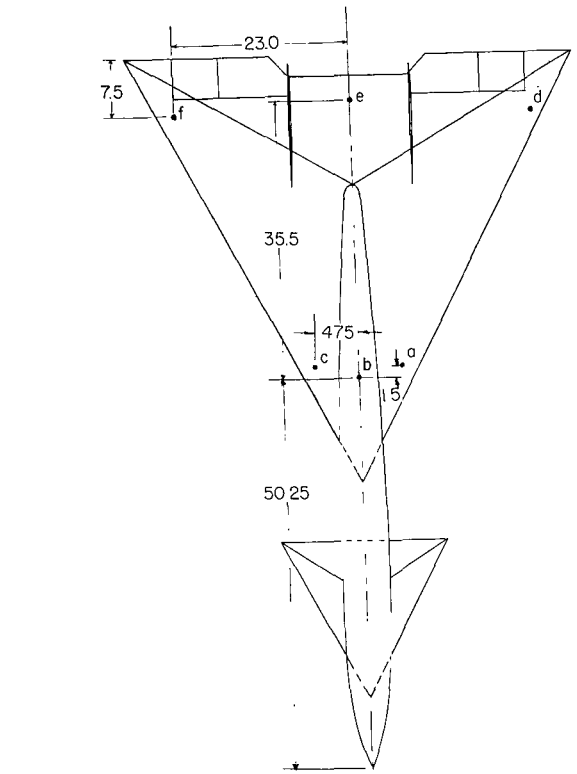

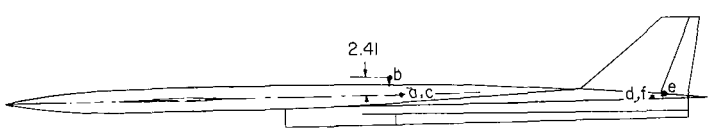

Location of parawing attachment points

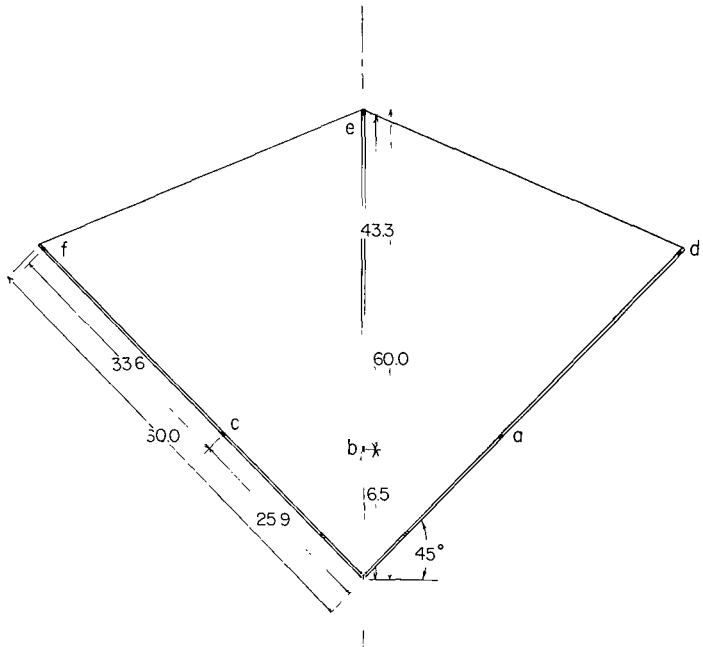

Parawing dimensional characteristics showing attachment points

(b) Parawing and riser attachment points.

Figure 3.- Concluded.

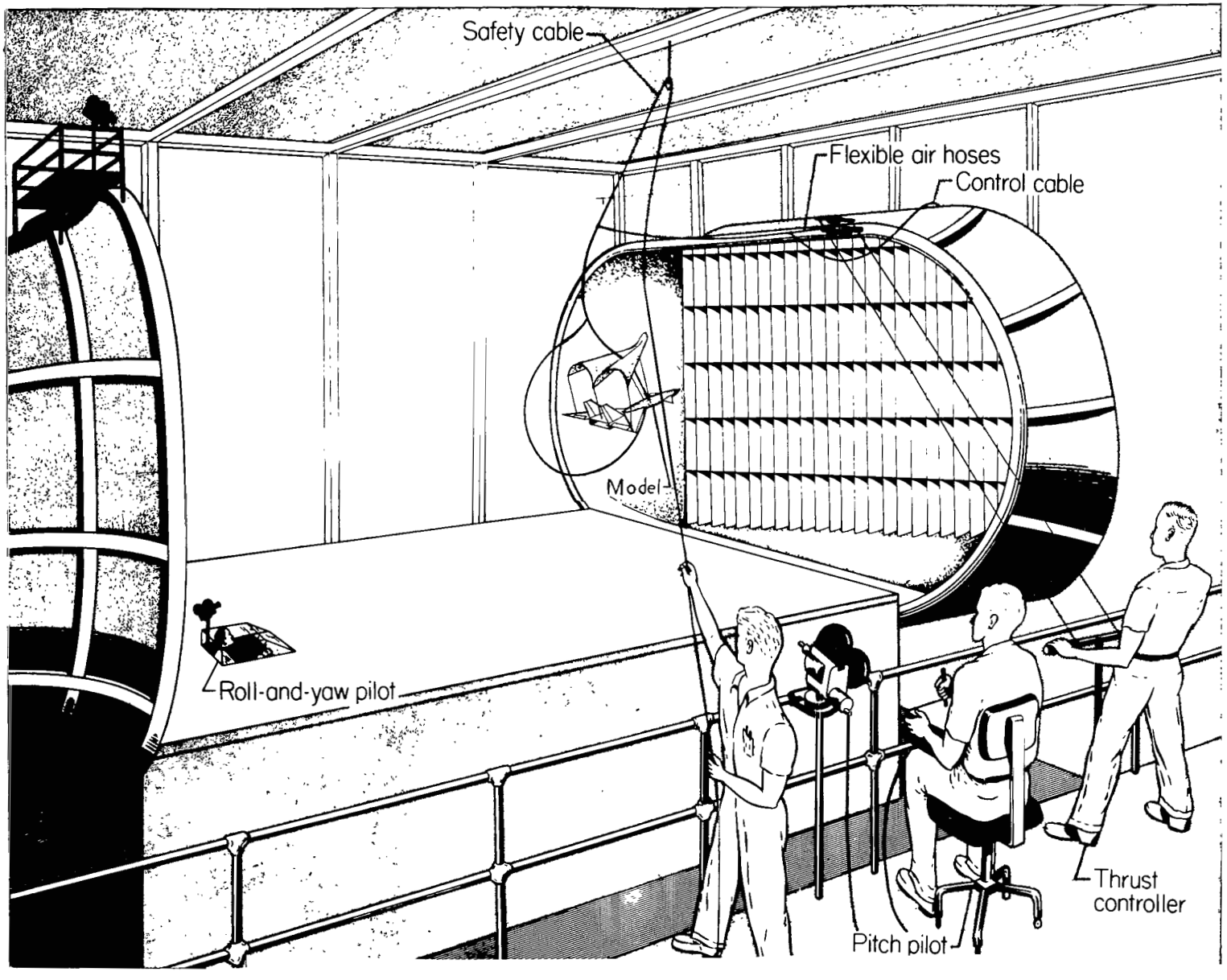

Figure 4.- Sketch of flight-test setup in the Langley full-scale tunnel.

L-60-2517

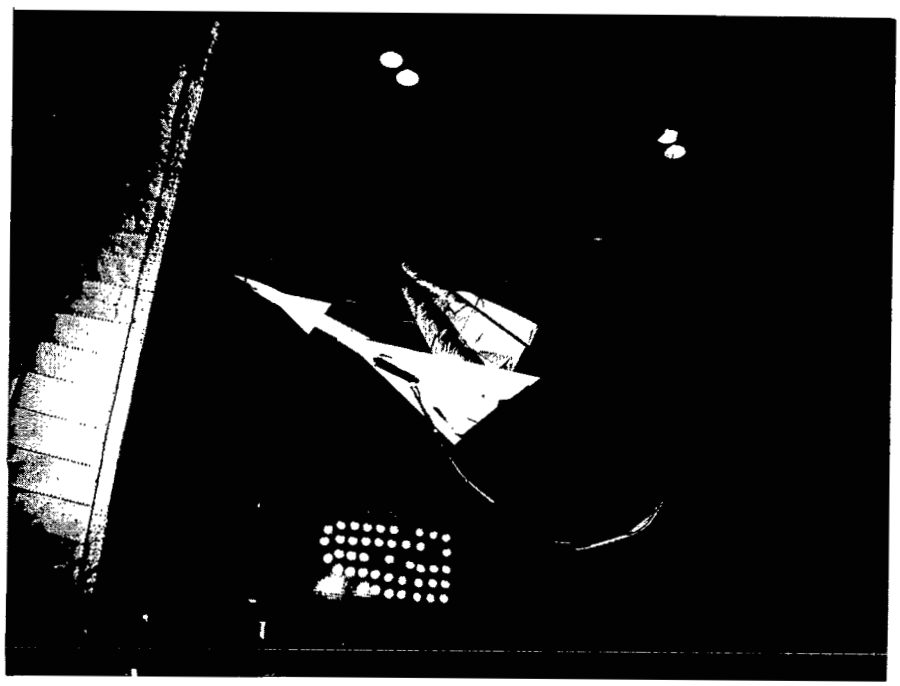

L-60-2518

Figure 5.- Model-parawing combination flying in the Langley full-scale tunnel.

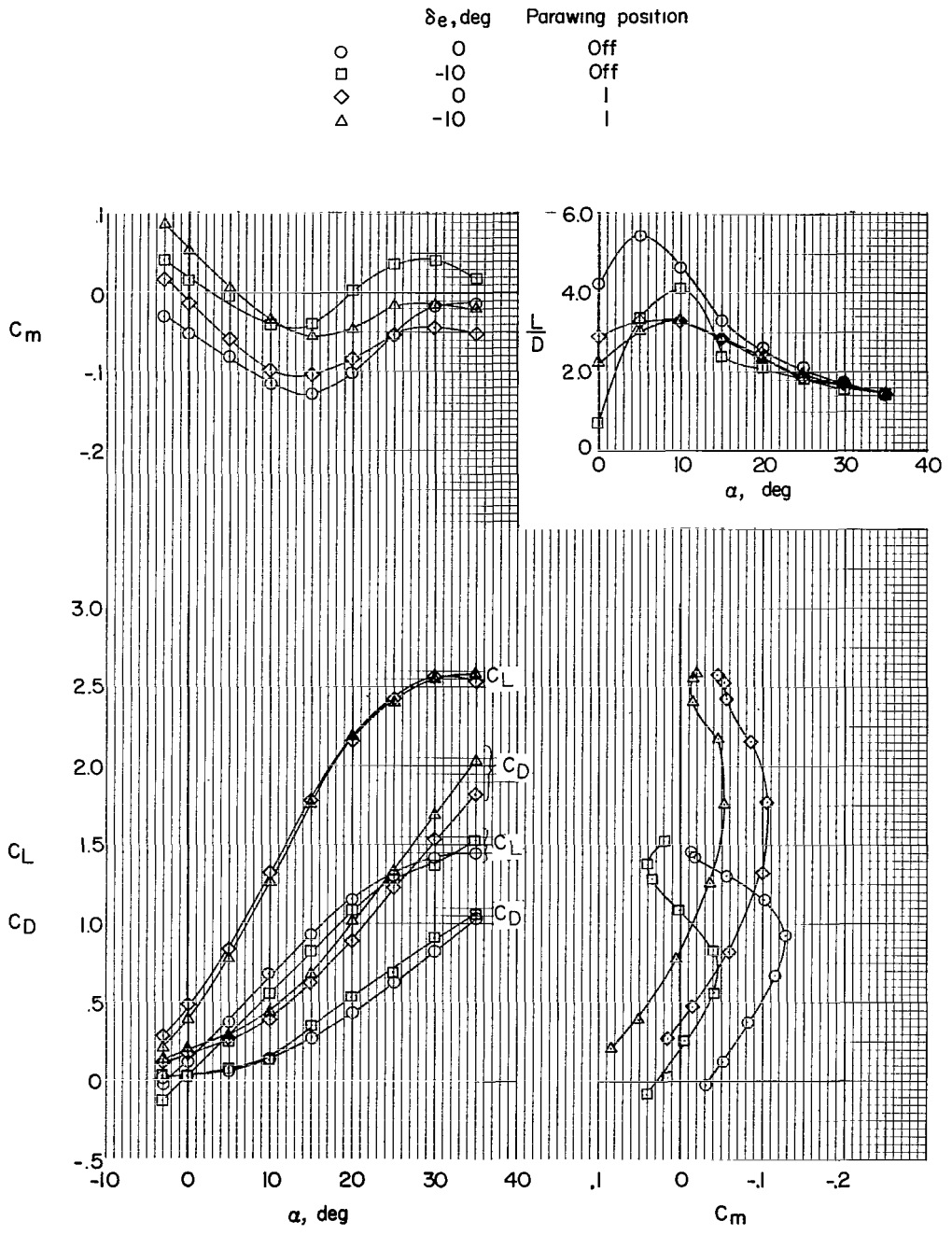

(a) Parawing position 1.

Figure 6.- Effect of the parawing on the static longitudinal stability characteristics of the model.

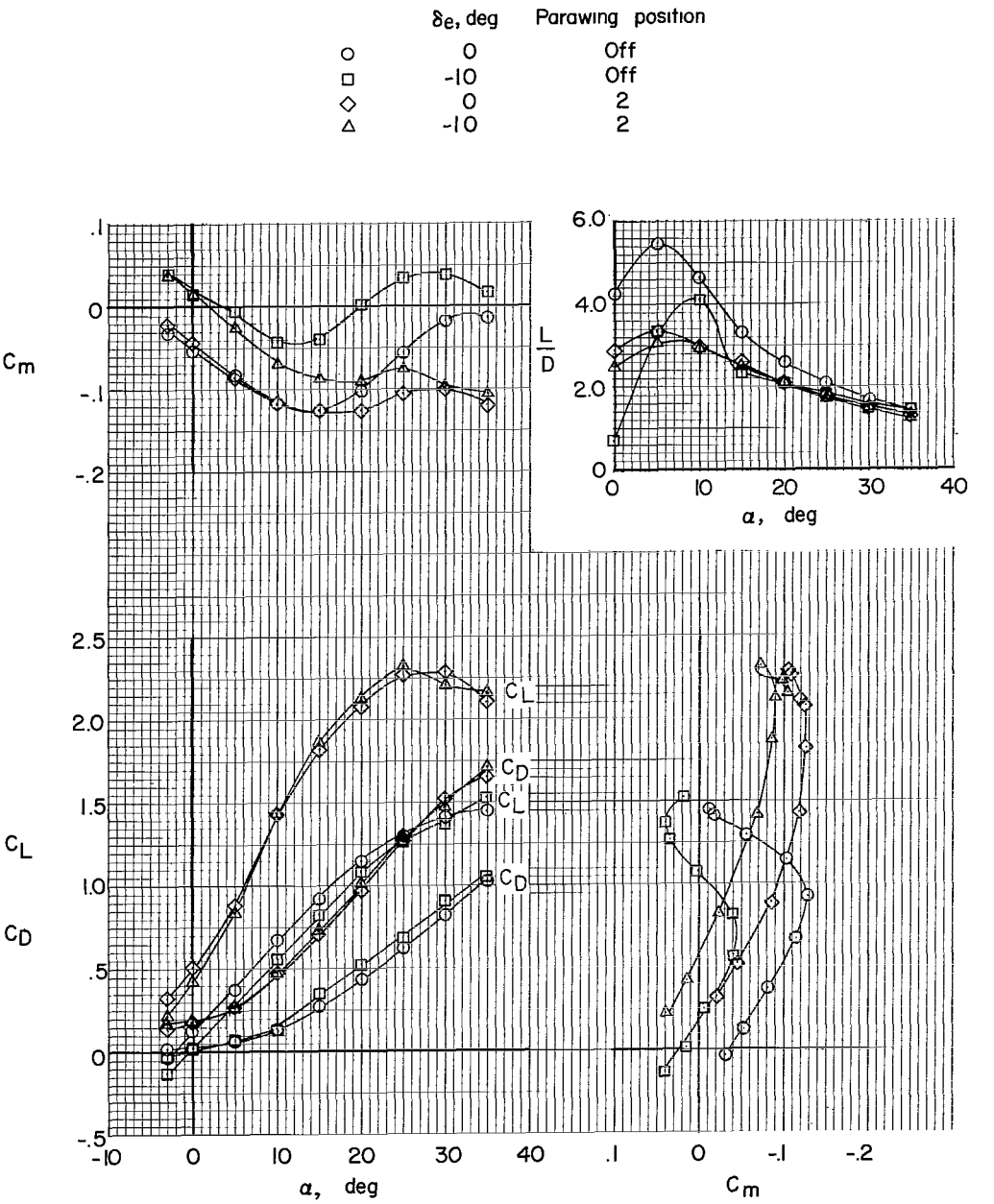

(b) Parawing position 2.

Figure 6.- Continued.

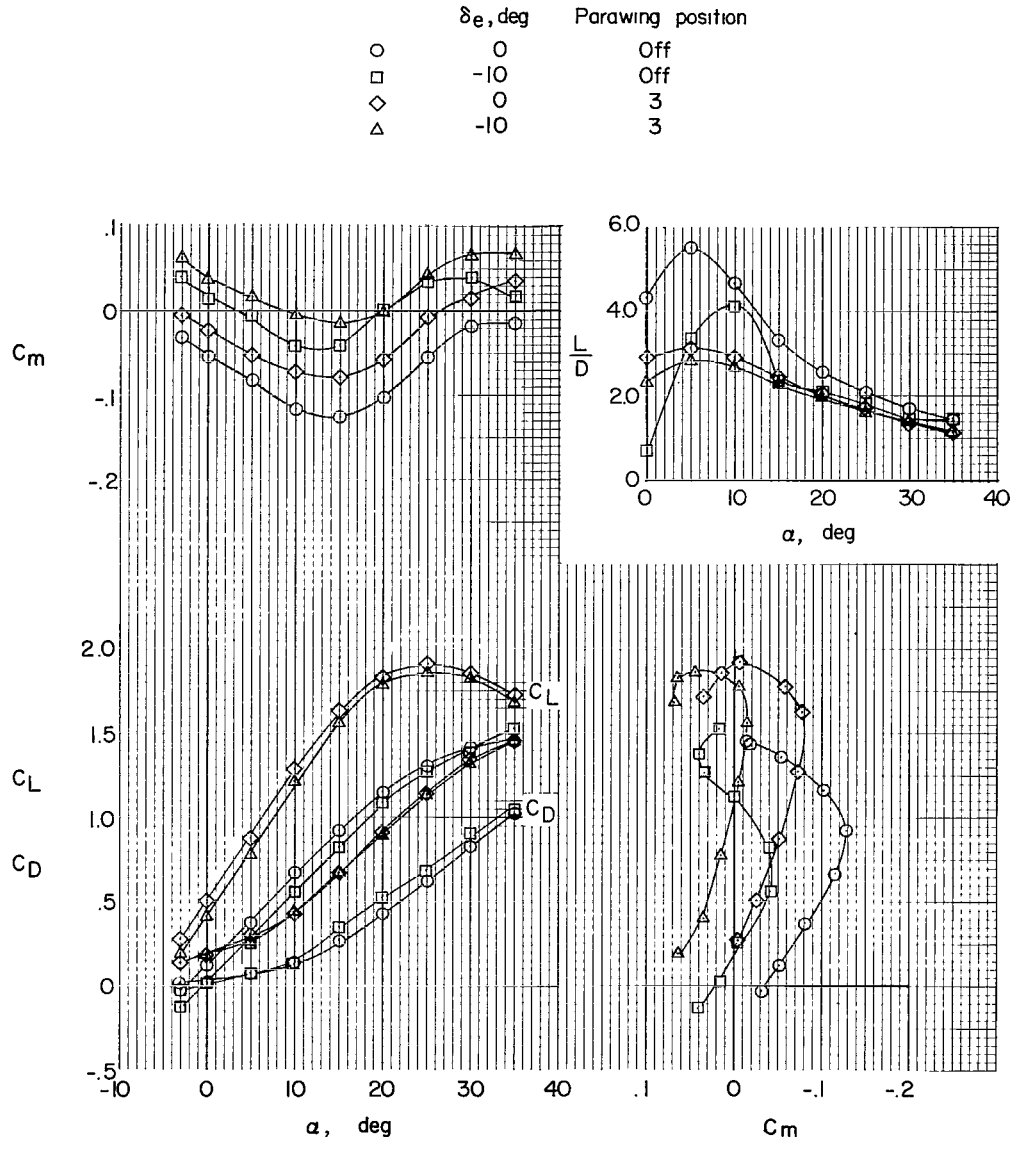

(c) Parawing position 3.

Figure 6.- Continued.

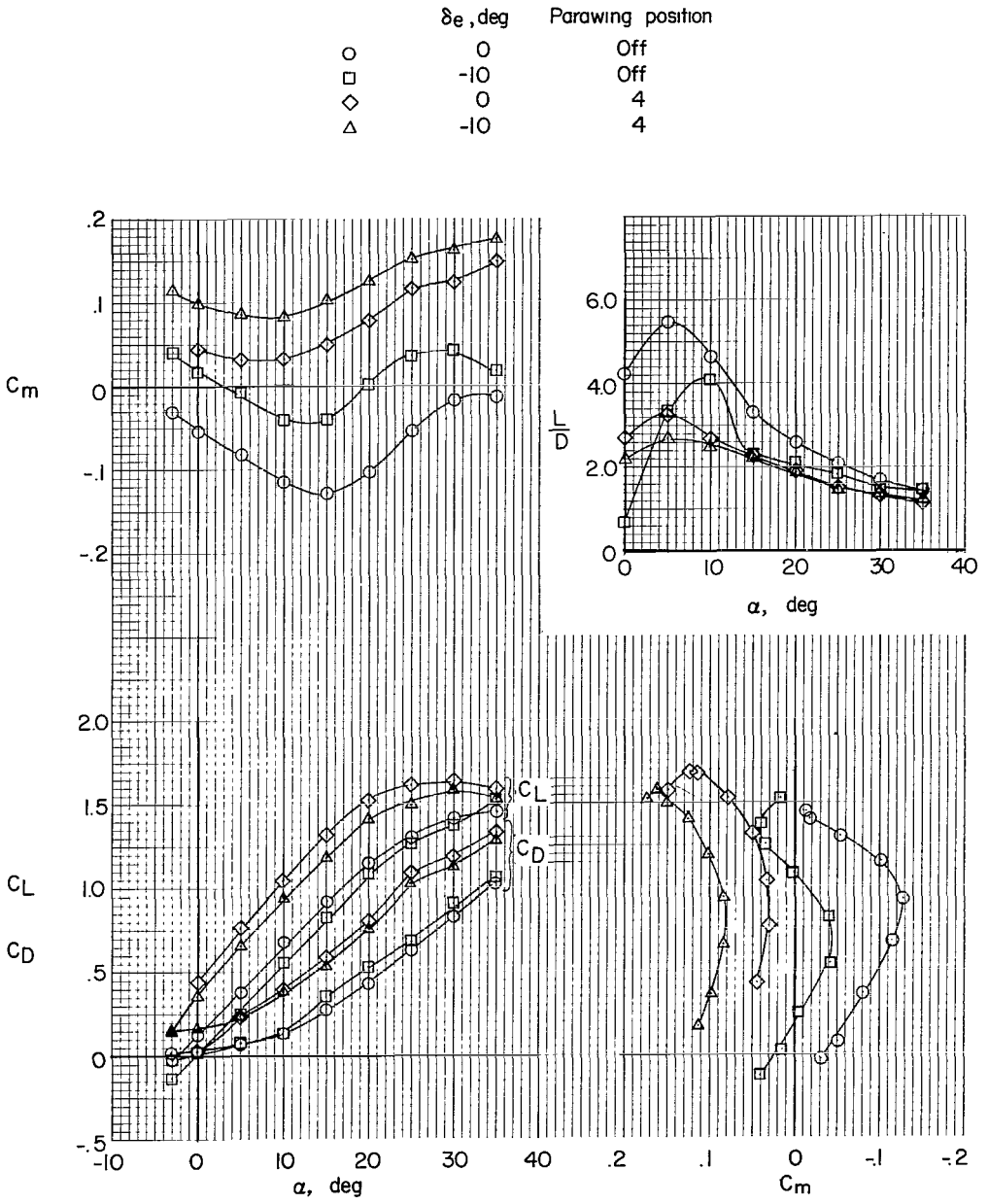

(d) Parawing position 4.

Figure 6.- Continued.

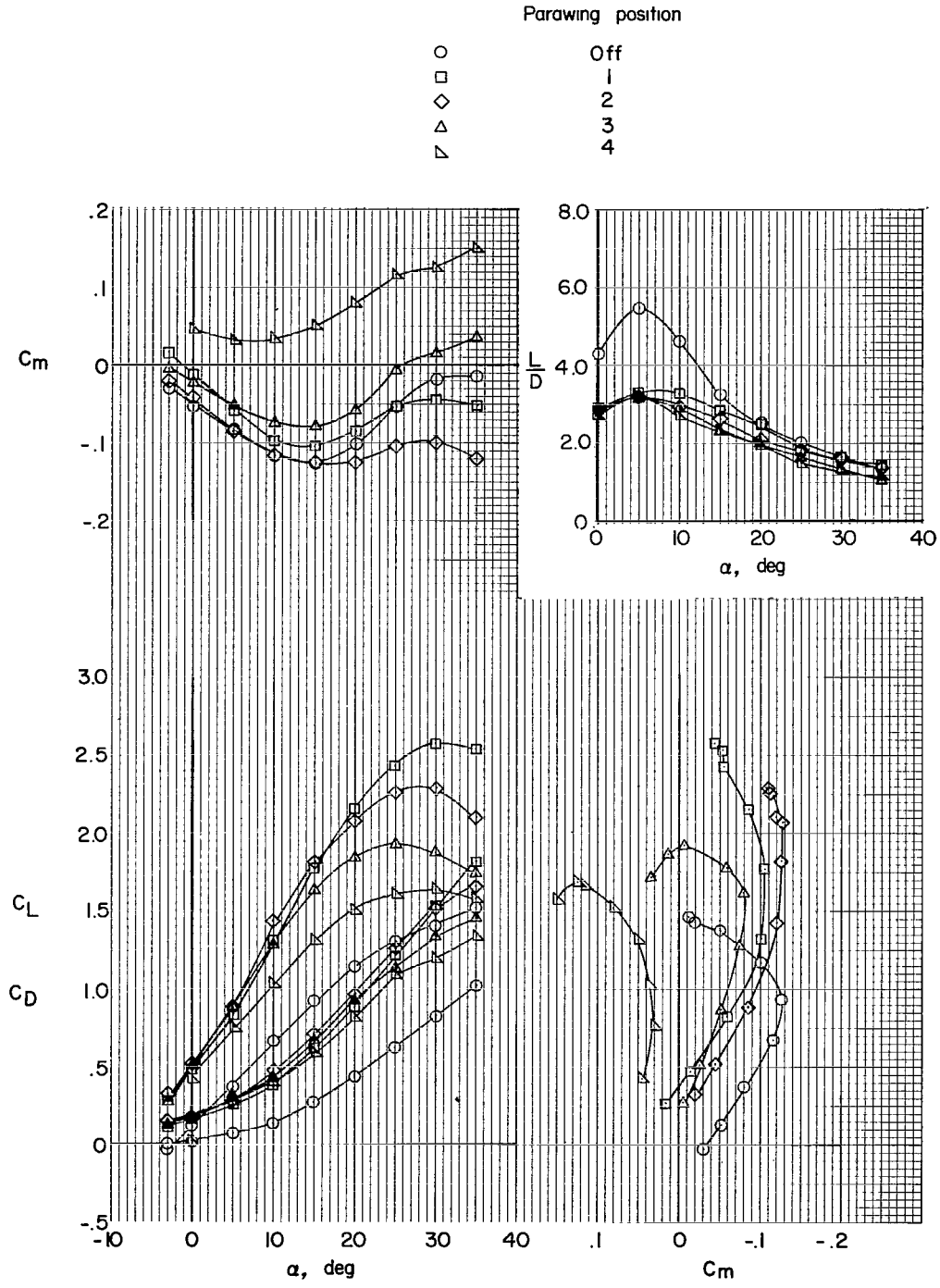

(e) Summary of parawing positions 1 to 4. $\delta_e = 0^o$.

Figure 6.- Concluded.

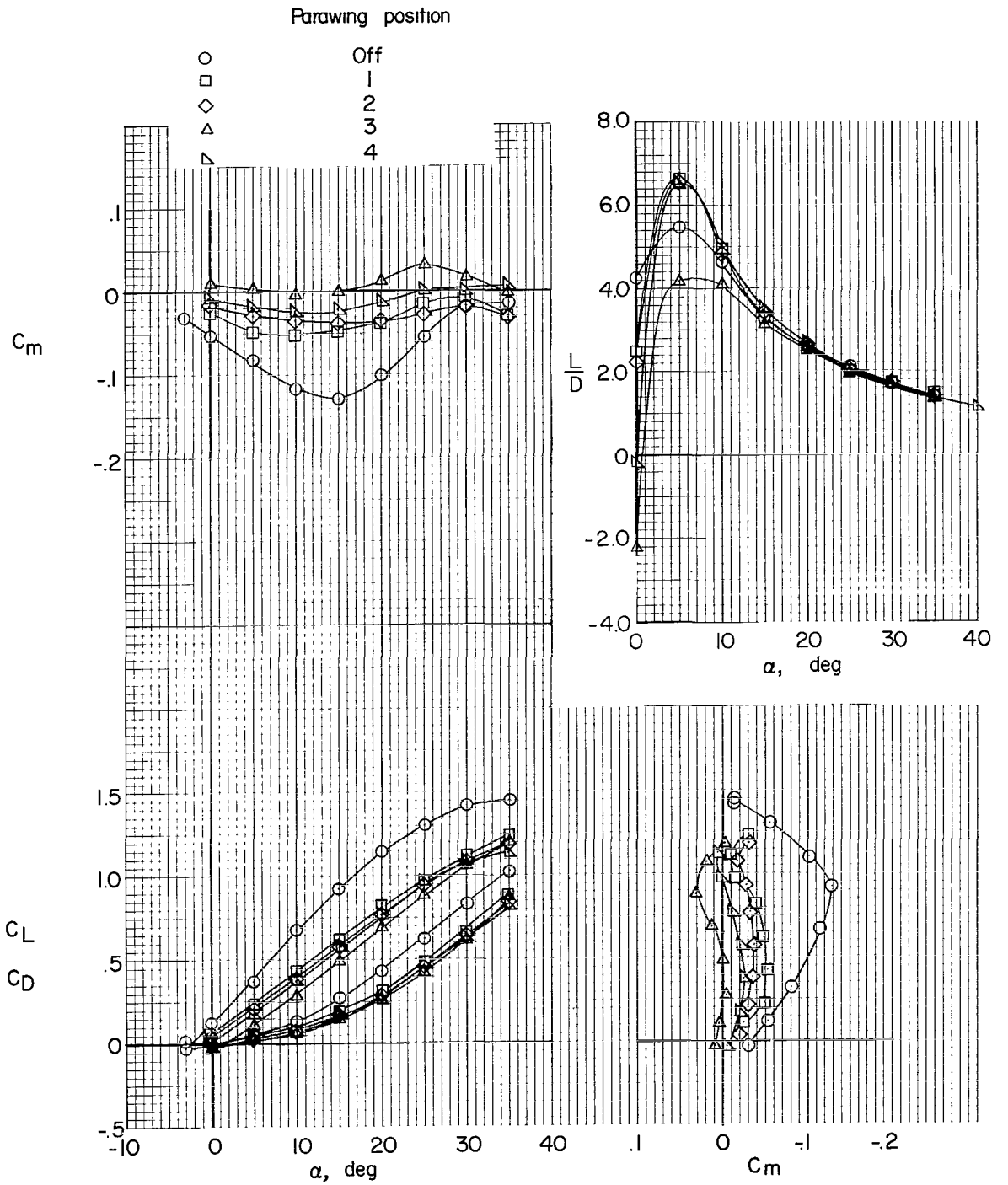

(a) Induced effects of the parawing.

Figure 7.- Static longitudinal stability characteristics of the model in the presence of the parawing. Parawing detached but located above the model in positions 1 to 4. $\delta_e = 0^o$.

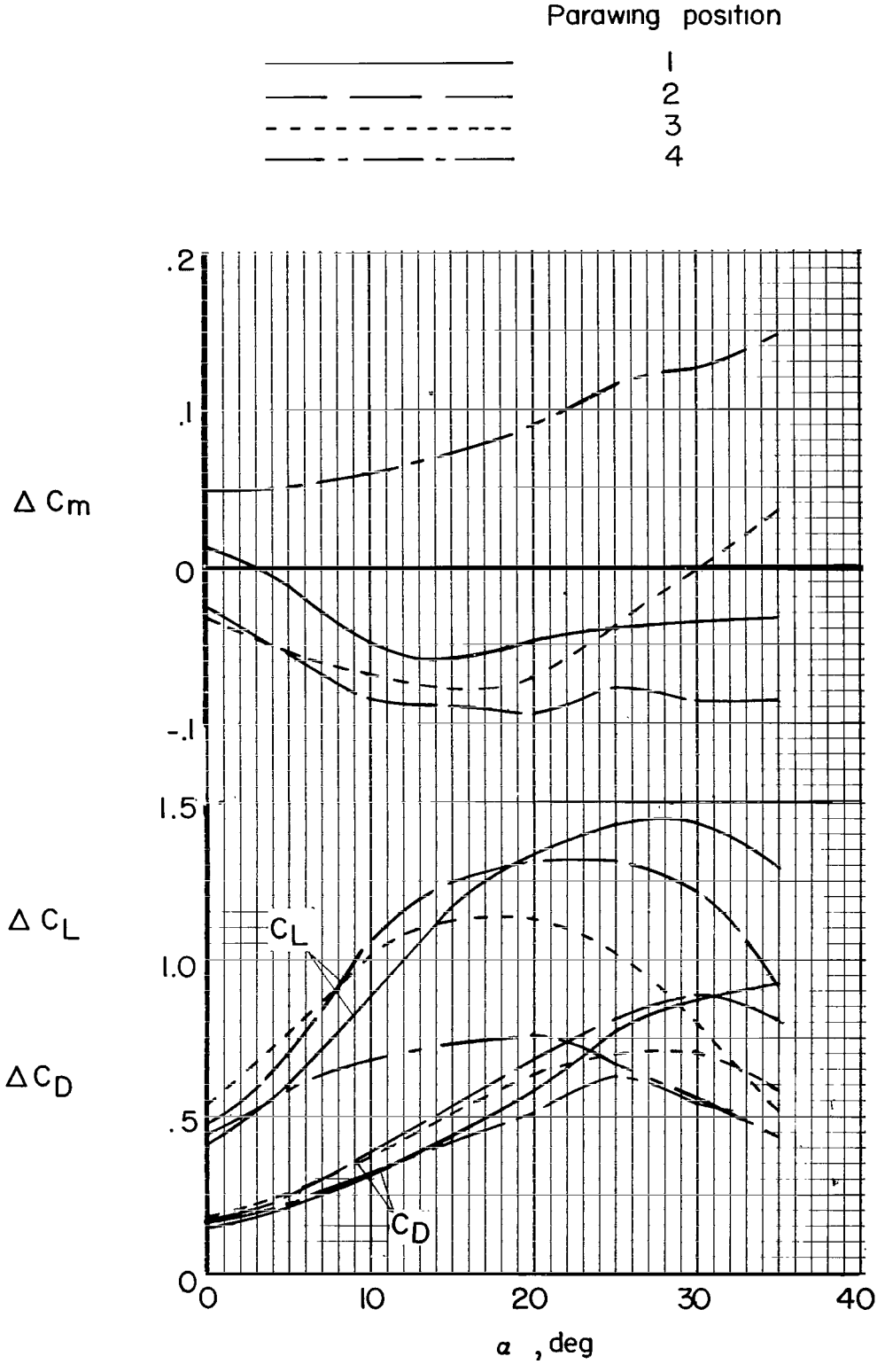

(b) Incremental longitudinal stability characteristics of the parawing obtained by subtracting data of figure 7(a) from figure 6(e).

Figure 7.- Concluded.

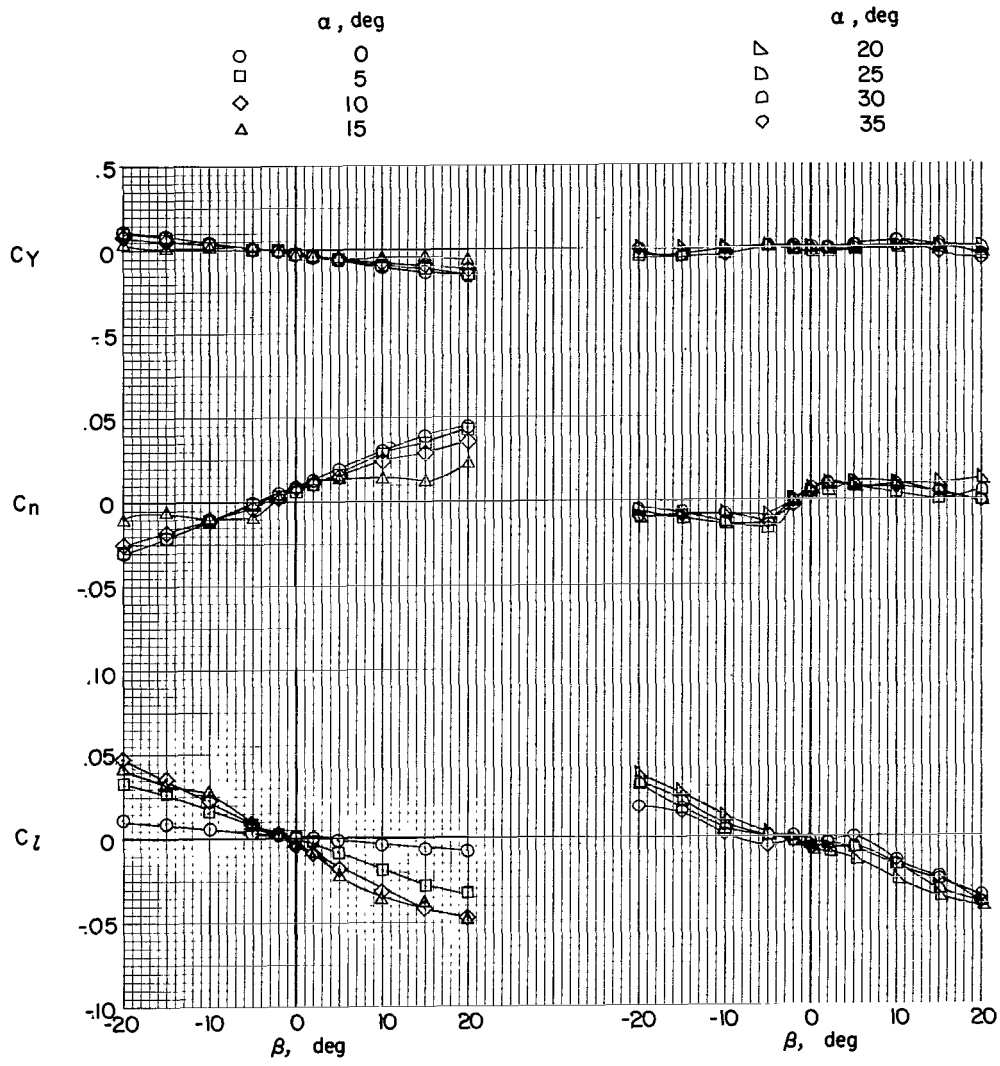

(a) Basic model.

Figure 8.- Effect of the parawing on the variation of the static lateral stability characteristics of the model with sideslip. $\delta_e = -10^\circ$.

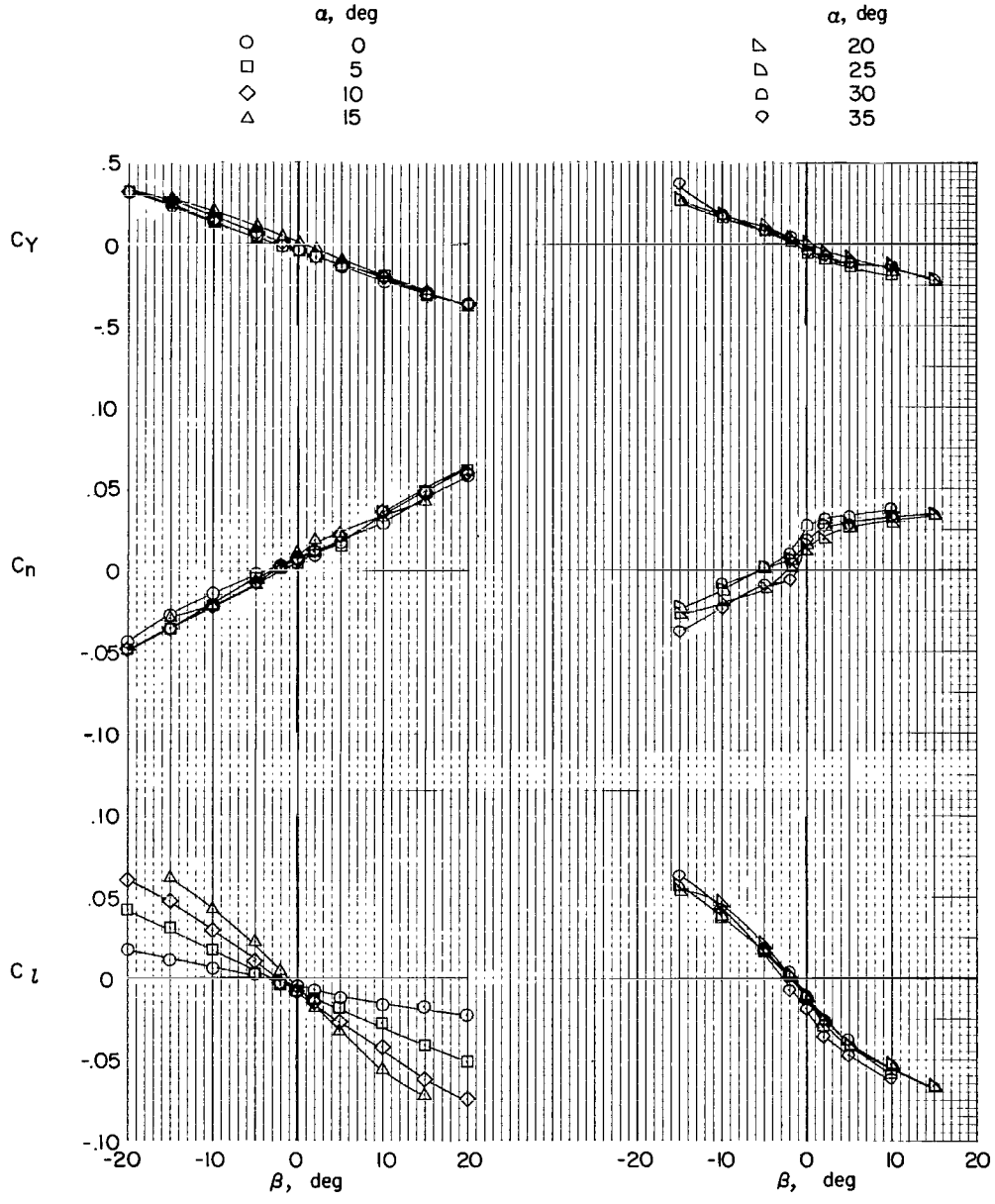

(b) Parawing position 1.

Figure 8.- Continued.

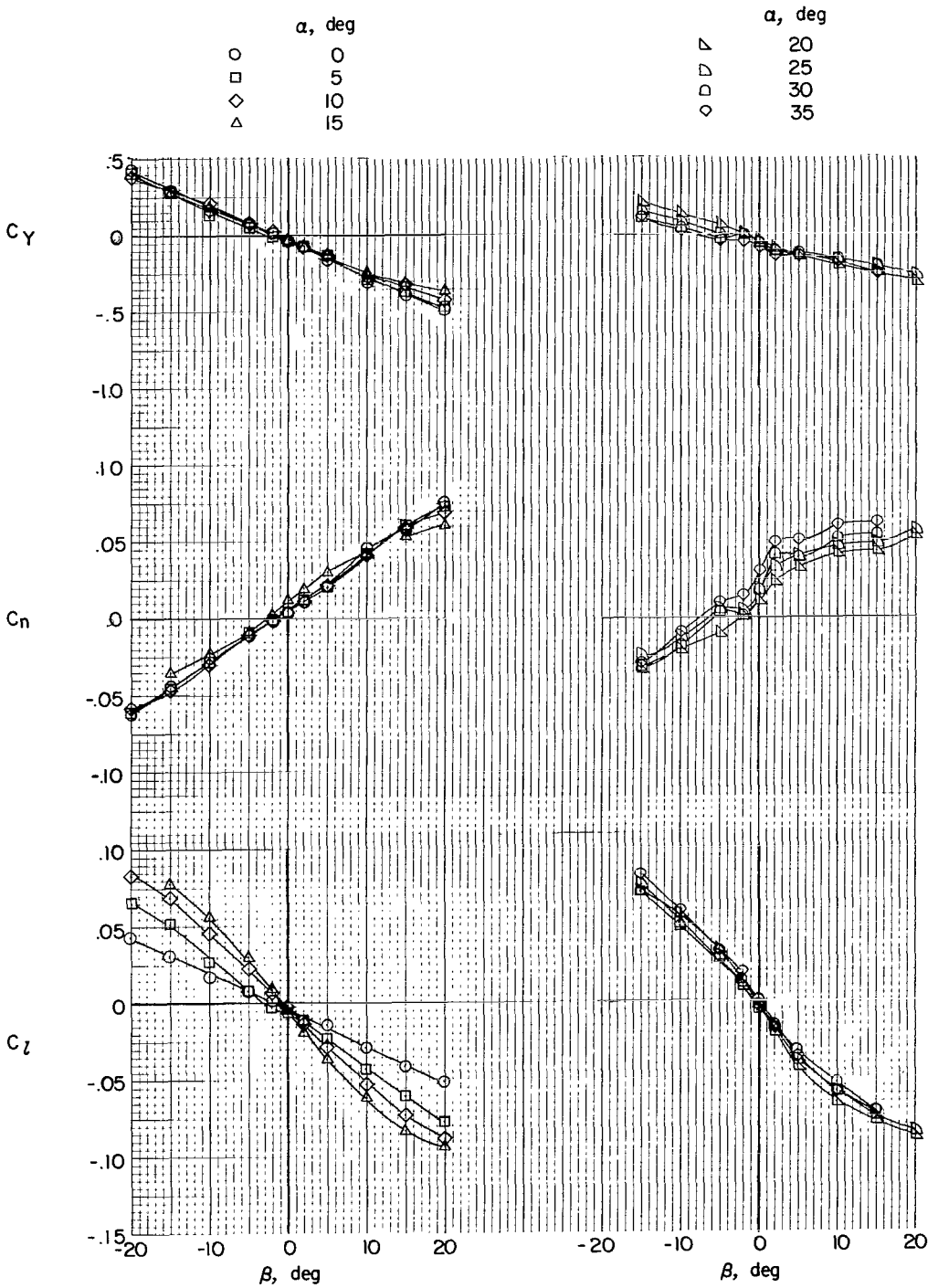

(c) Parawing position 2.

Figure 8.- Continued.

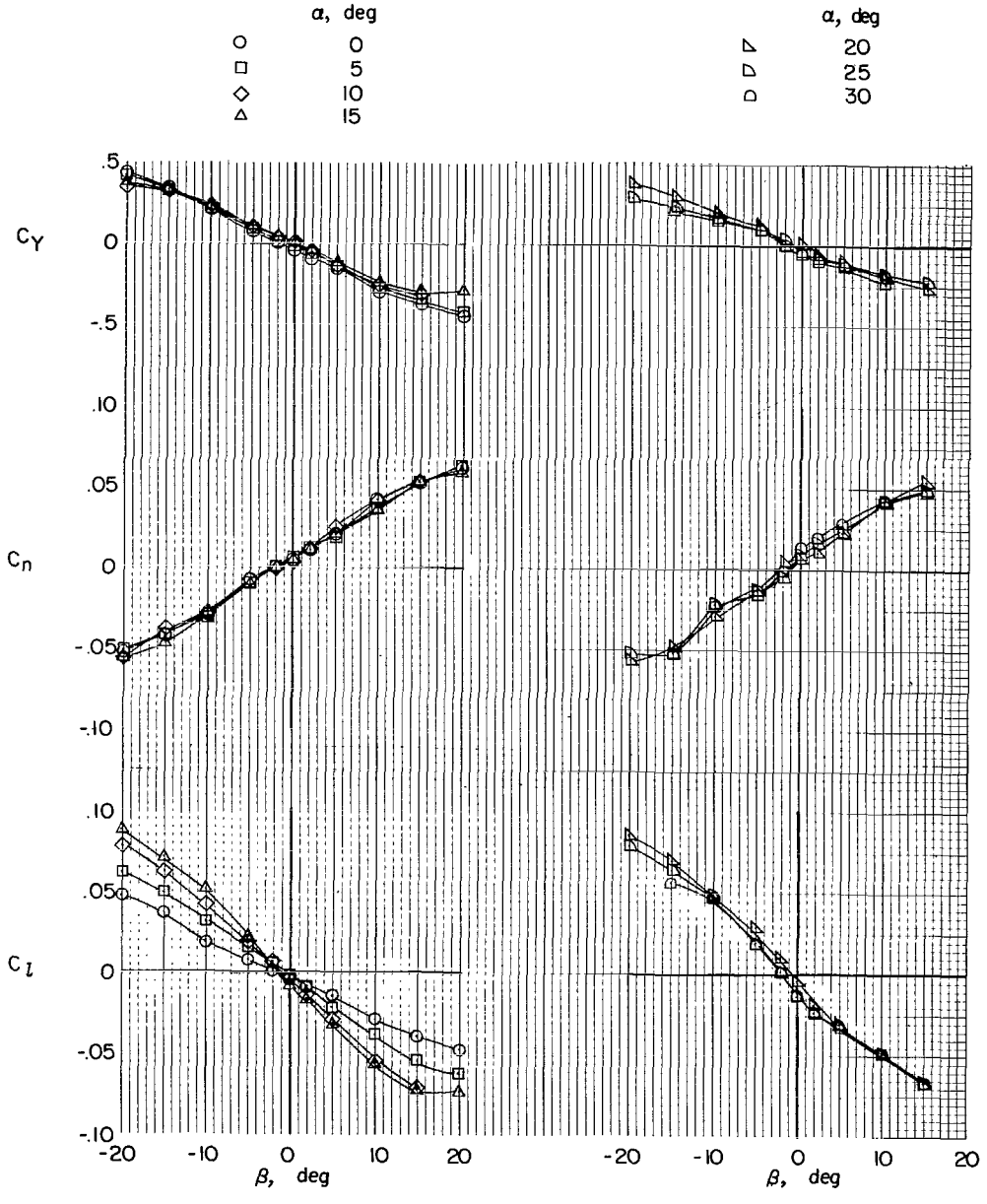

(d) Parawing position 3.

Figure 8.- Continued.

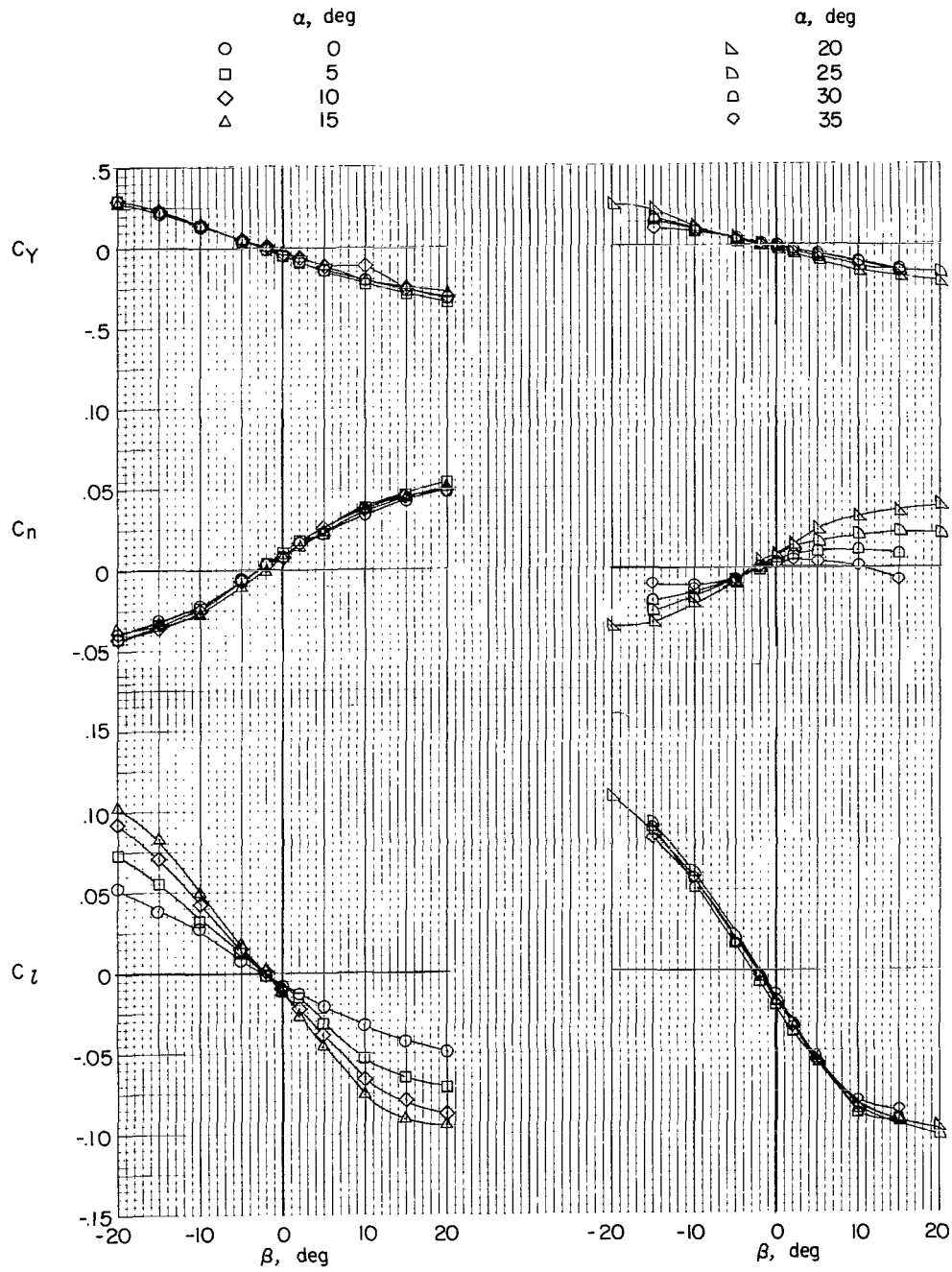

(e) Parawing position 4.

Figure 8.- Concluded.

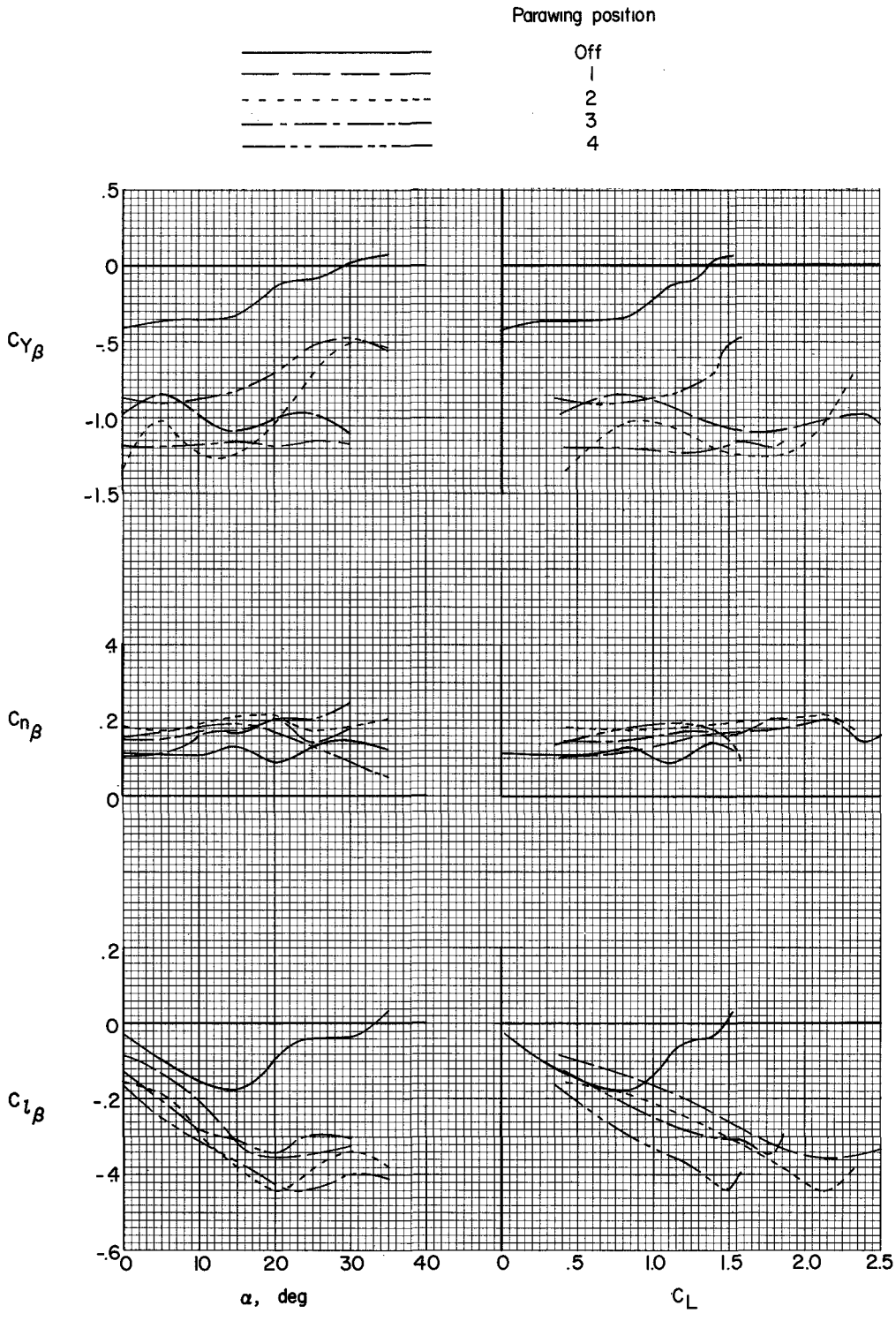

Figure 9.- Effect of the parawing on the static lateral stability parameters of the model. (Data obtained for $\beta = \pm 5^\circ$ from figure 8.)

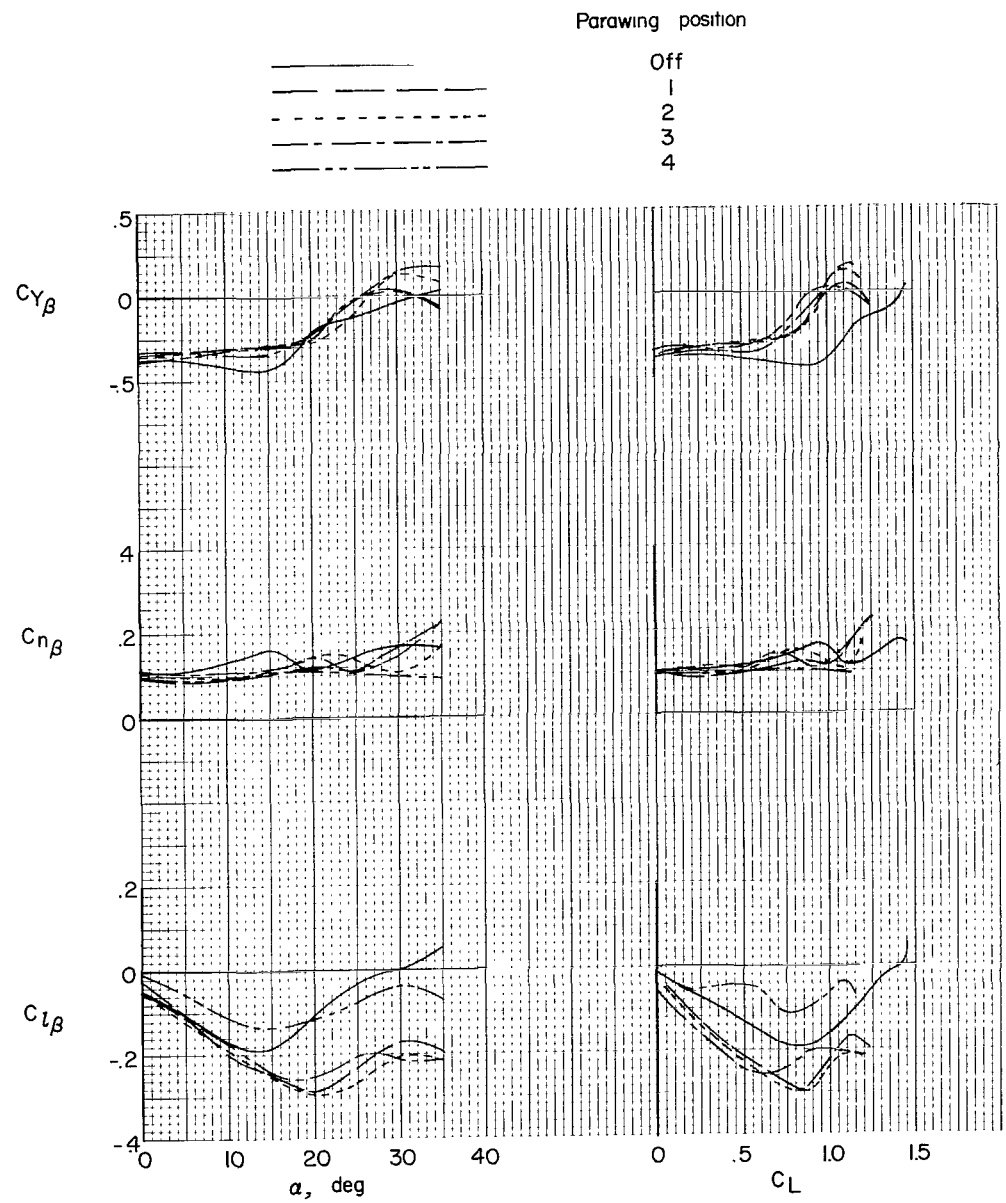

Figure 10.- Static lateral stability characteristics of the model in the presence of the parawing. Parawing detached but located above the model in positions 1 to 4.

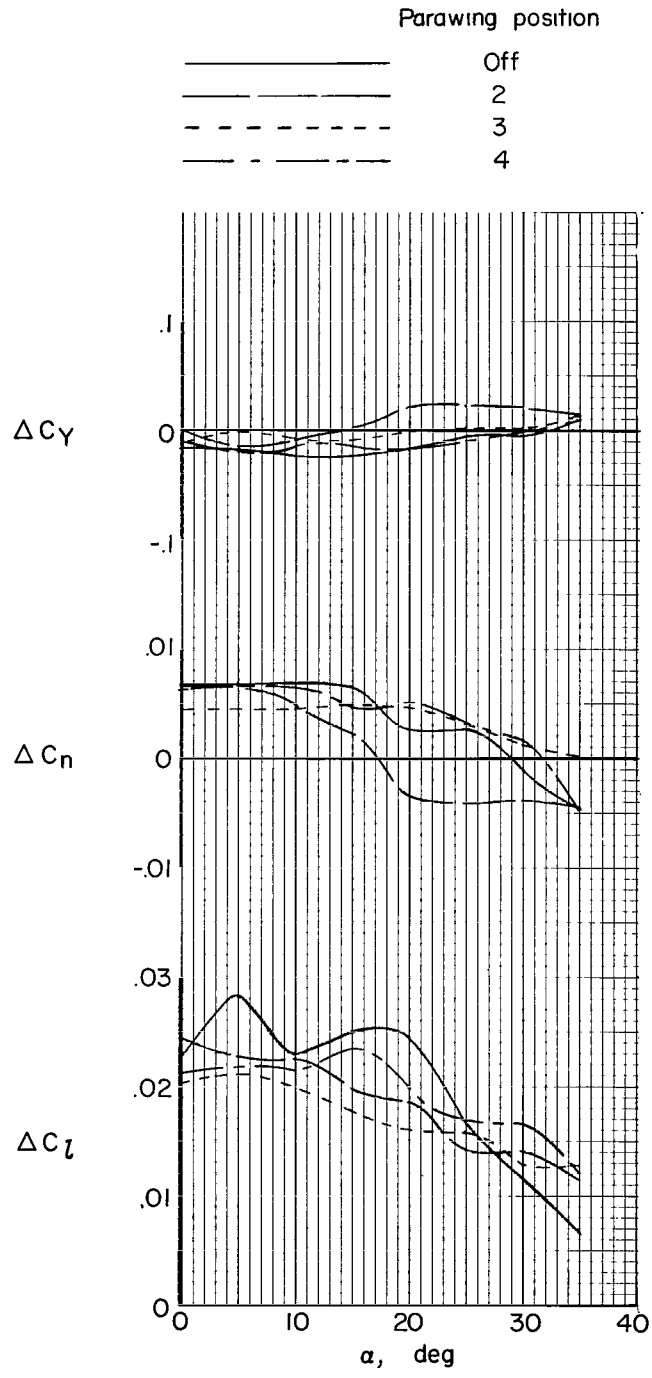

(a) Elevons deflected for roll control. $\delta_{e,left} = 12^{o}$; $\delta_{e,right} = -12^{o}$.

Figure 11.- Effect of the parawing on the static lateral control characteristics of the model. Large surfaces.

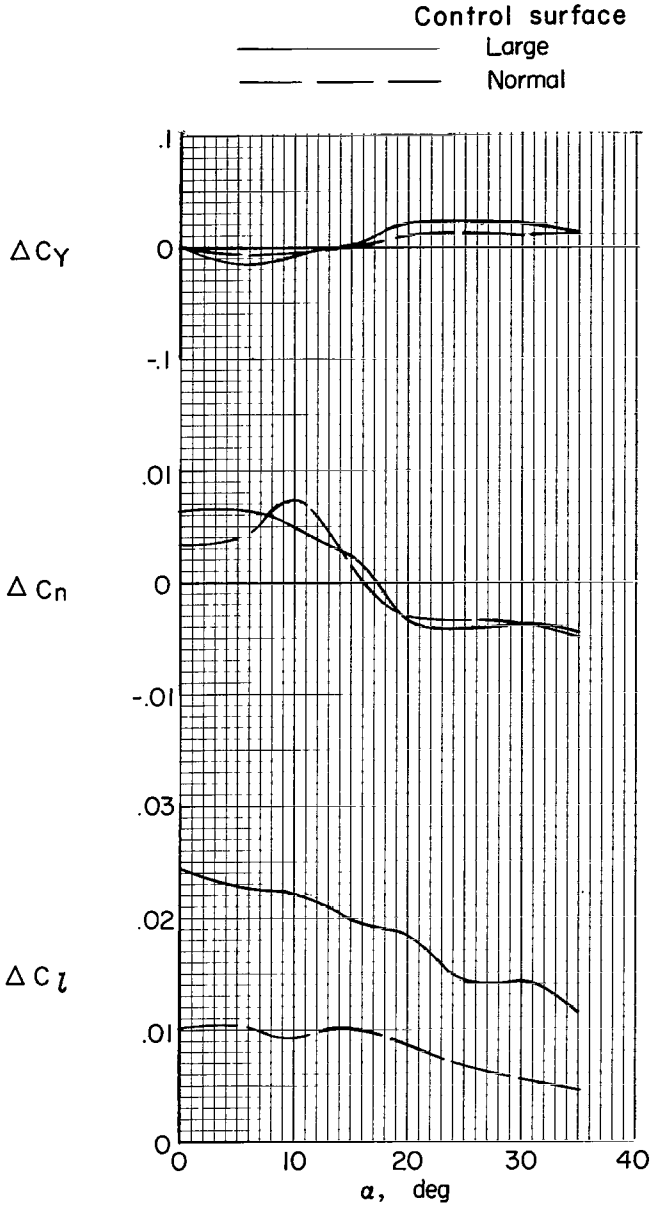

(b) Comparison of the rolling-moment effectiveness of basic and large control surfaces. Parawing in position 2. $\delta_{e,left} = 12^{o}$; $\delta_{e,right} = -12^{o}$.

Figure 11.- Continued.

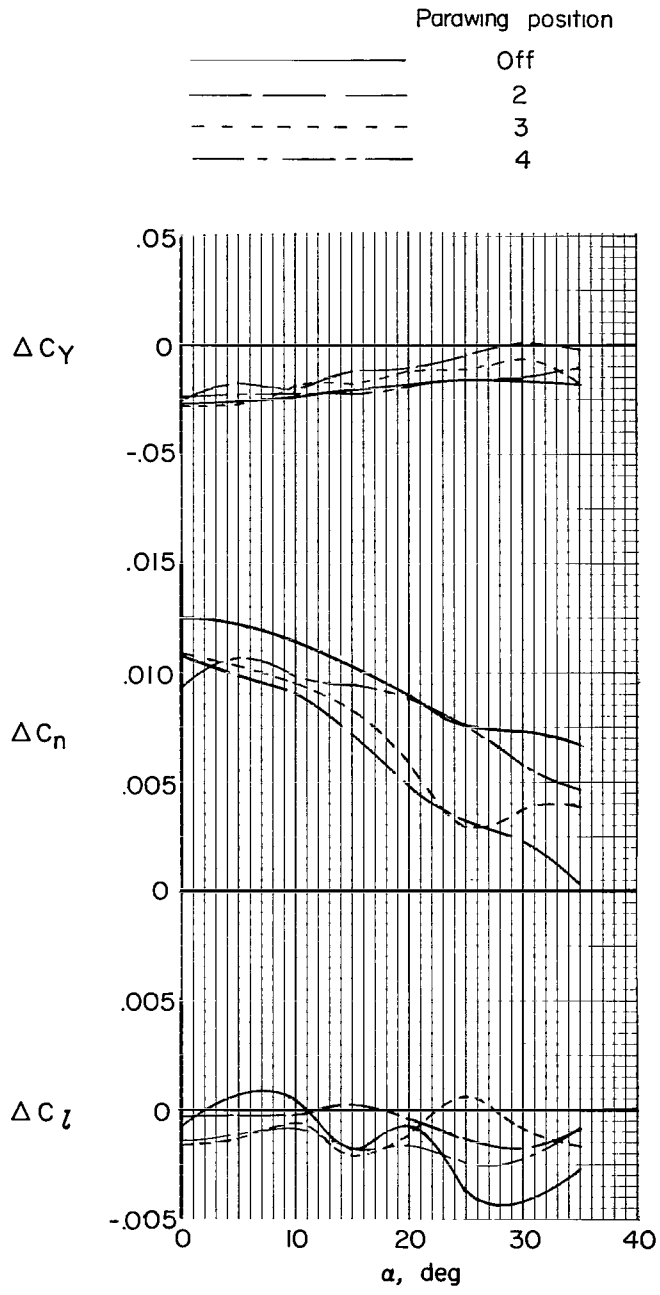

(c) Rudder effectiveness. $\delta_r = 10^\circ$ right (both surfaces).

Figure 11.- Concluded.

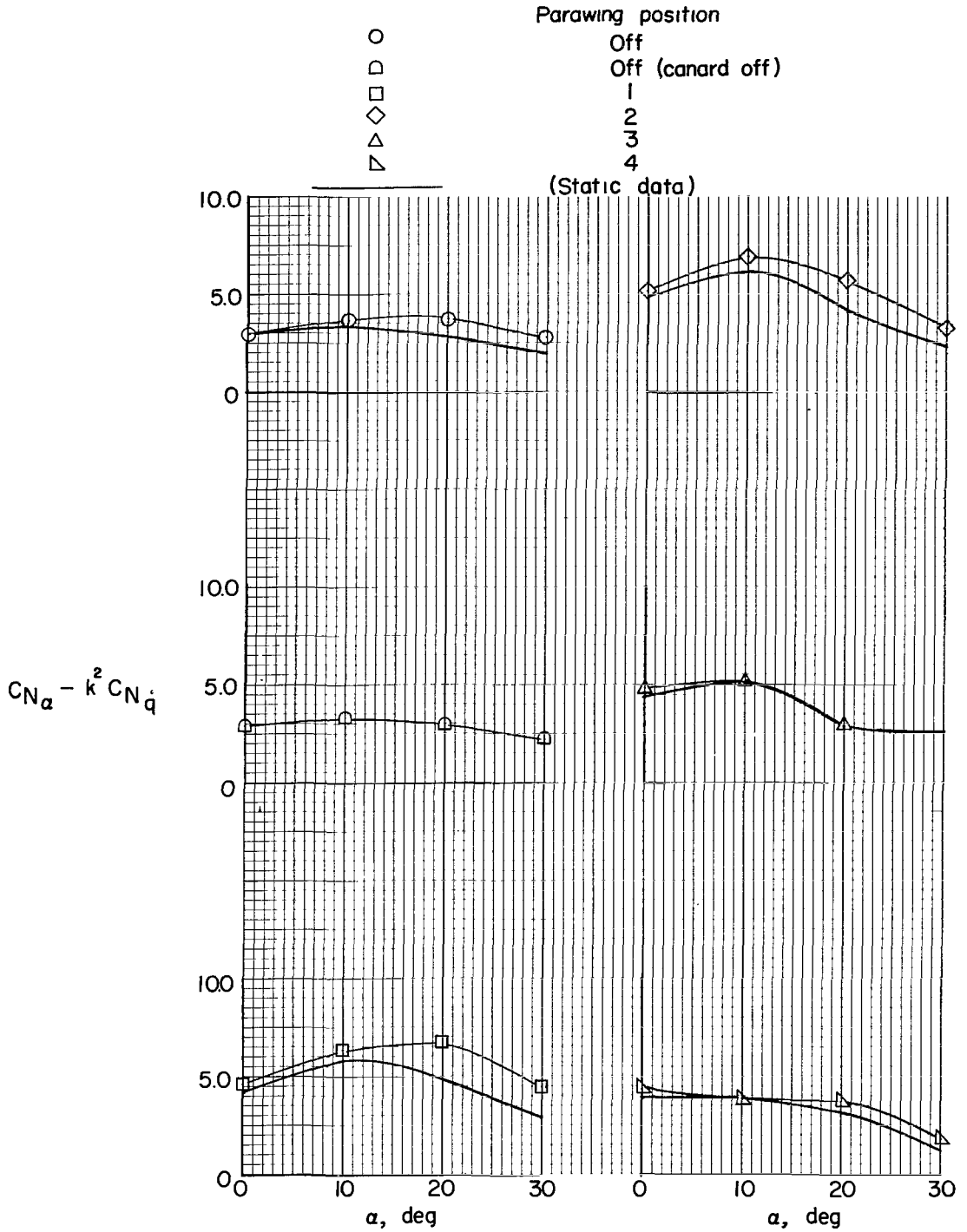

(a) Normal-force coefficient.

Figure 12.- Effect of the parawing on the in-phase pitching-oscillation derivatives of the model.

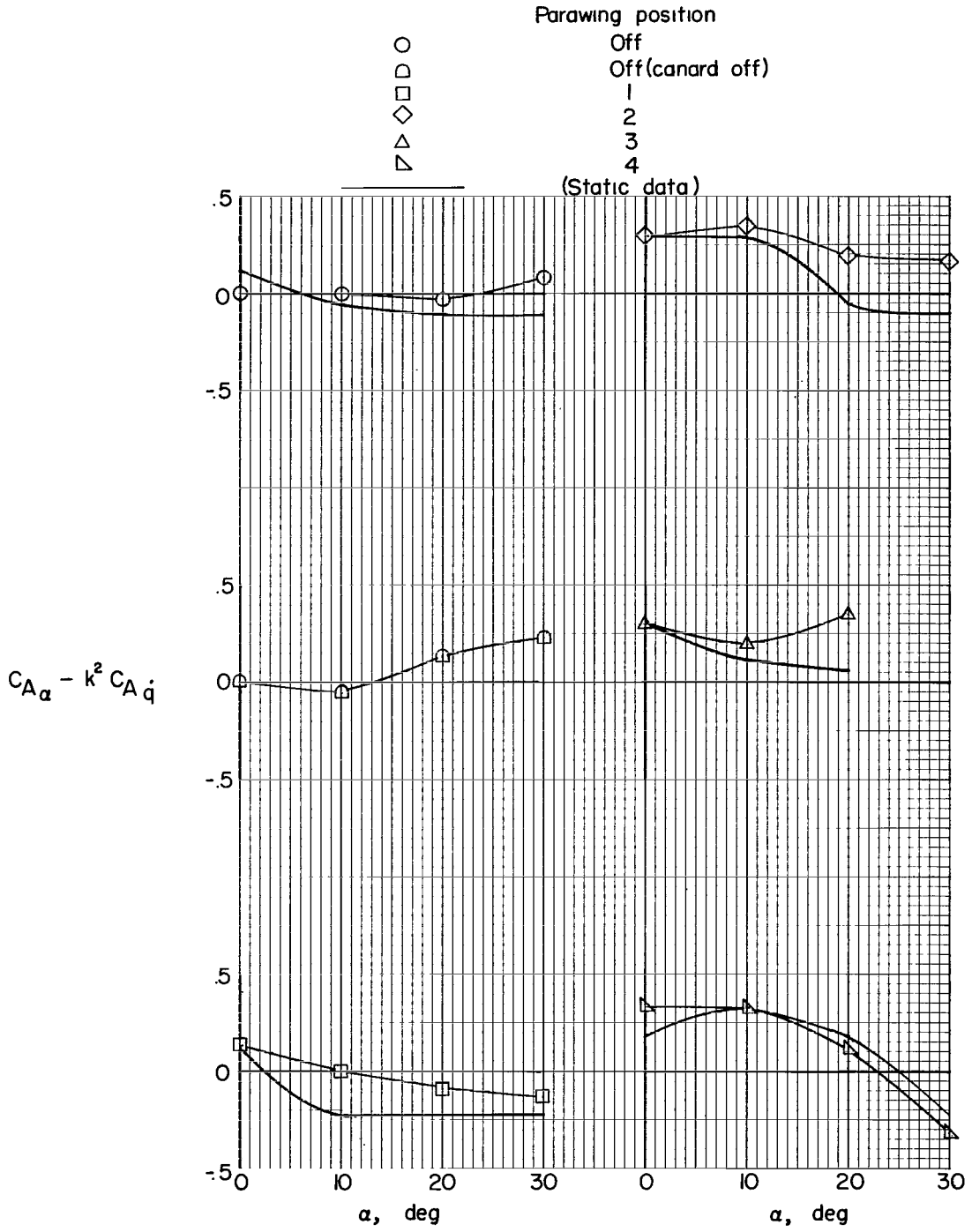

(b) Axial-force coefficient.

Figure 12.- Continued.

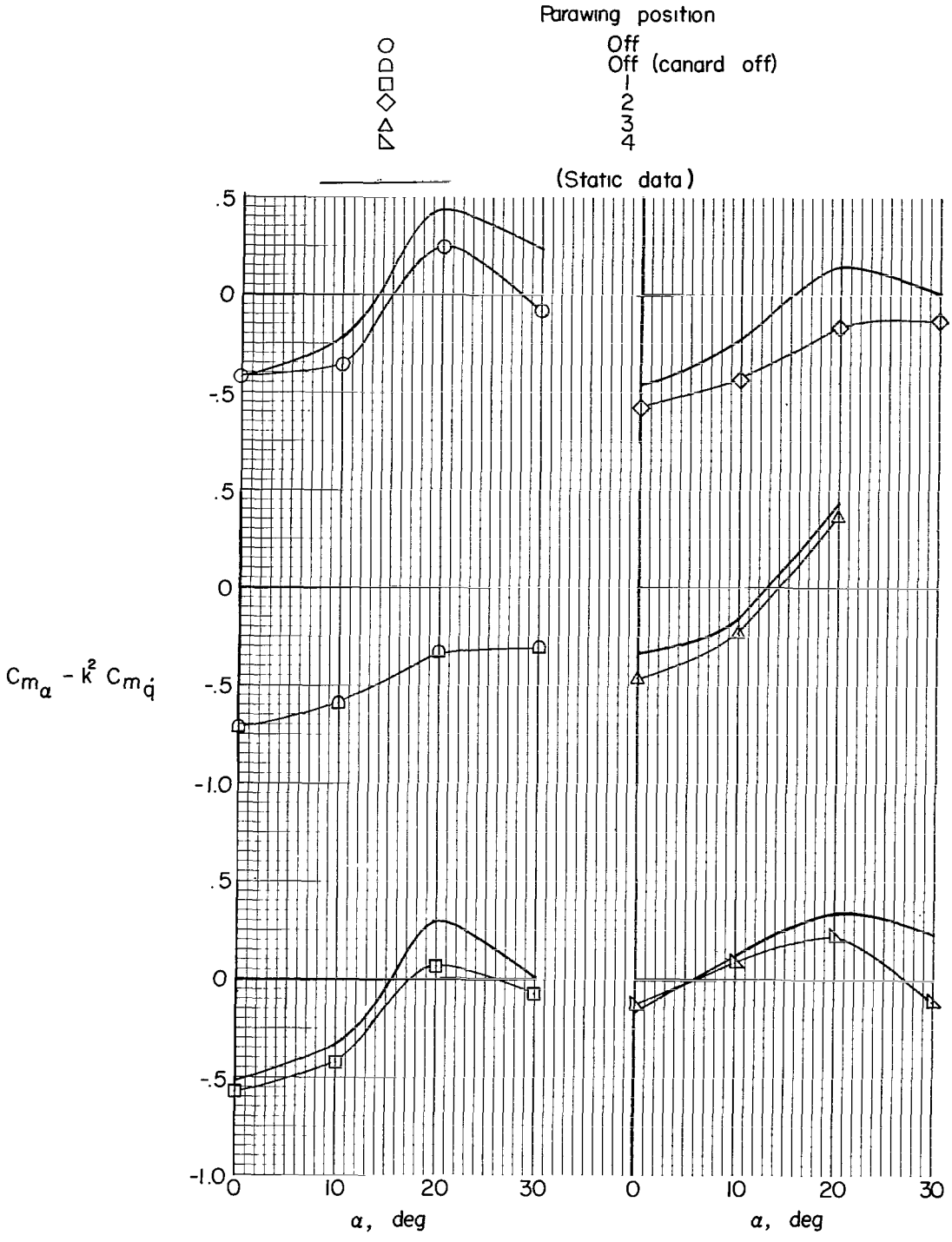

(c) Pitching-moment coefficient.

Figure 12.- Concluded.

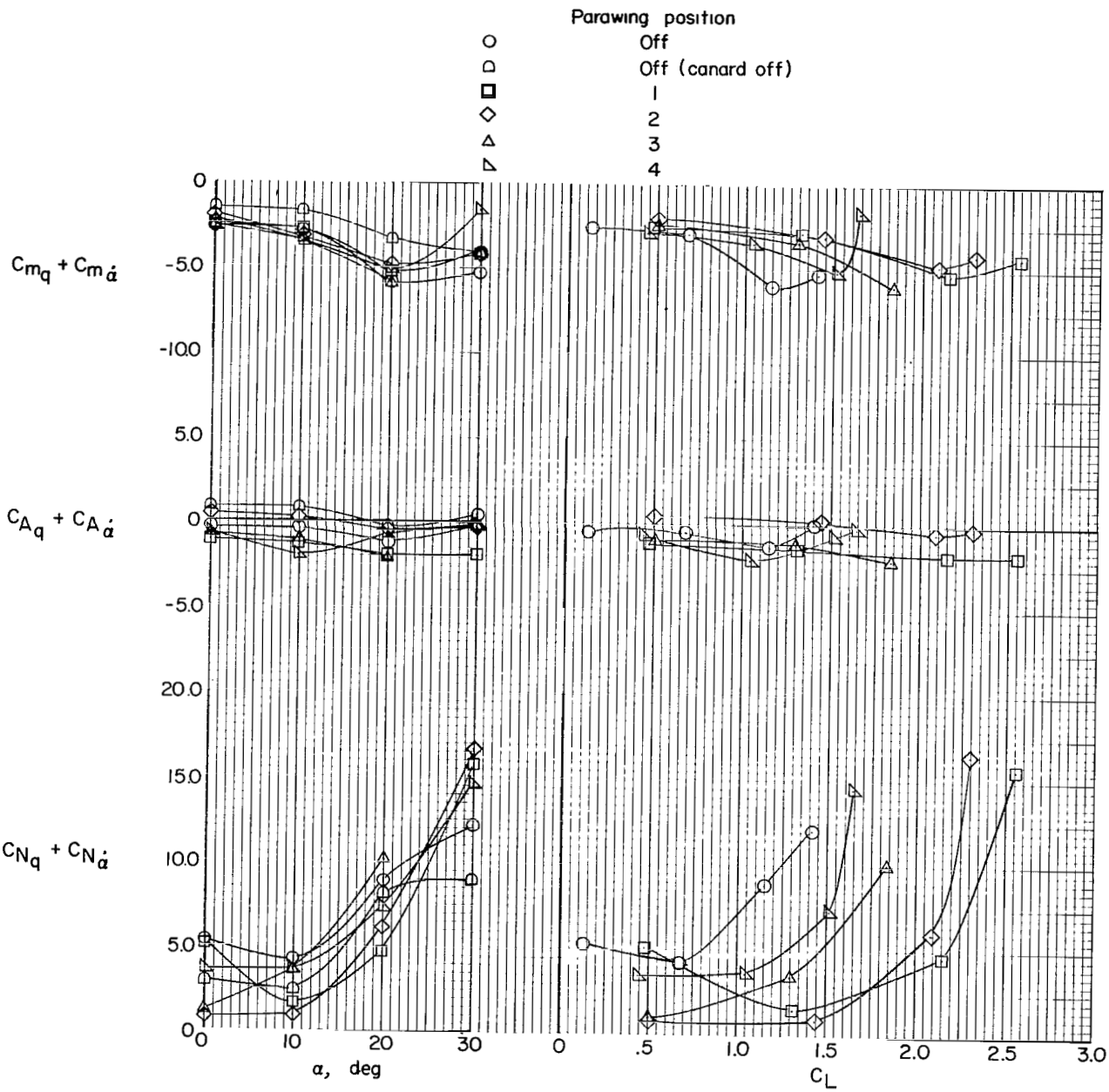

Figure 13.- Effect of the parawing on the out-of-phase pitching-oscillation derivatives of the model.

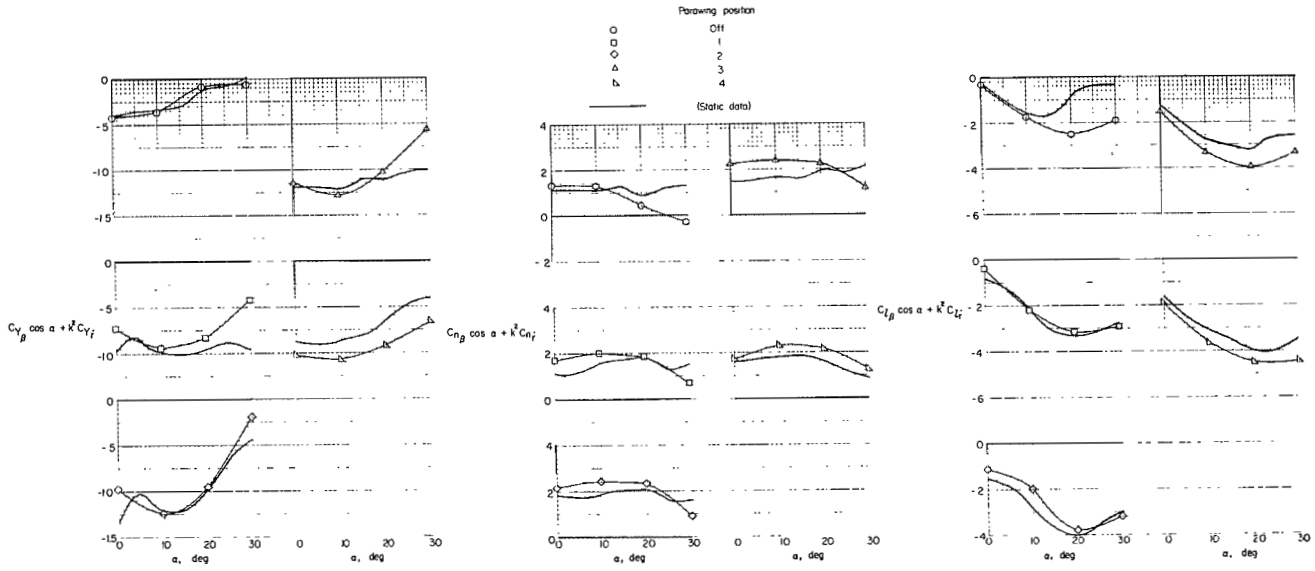

(a) In-phase yawing derivatives.

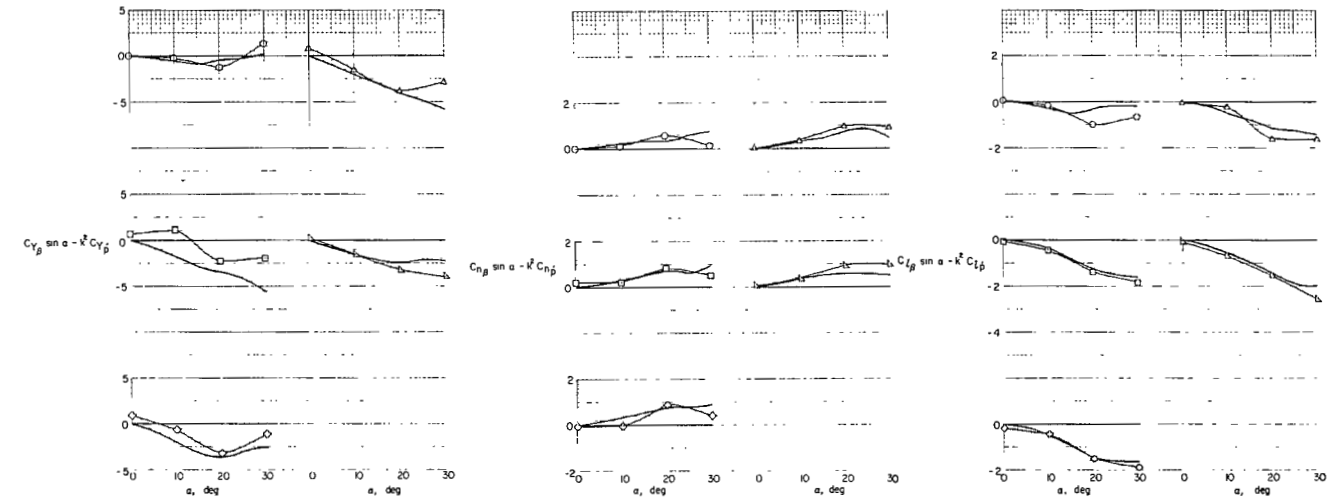

(b) In-phase rolling derivatives.

Figure 14.- Effect of the parawing on the in-phase lateral oscillatory derivatives of the model.

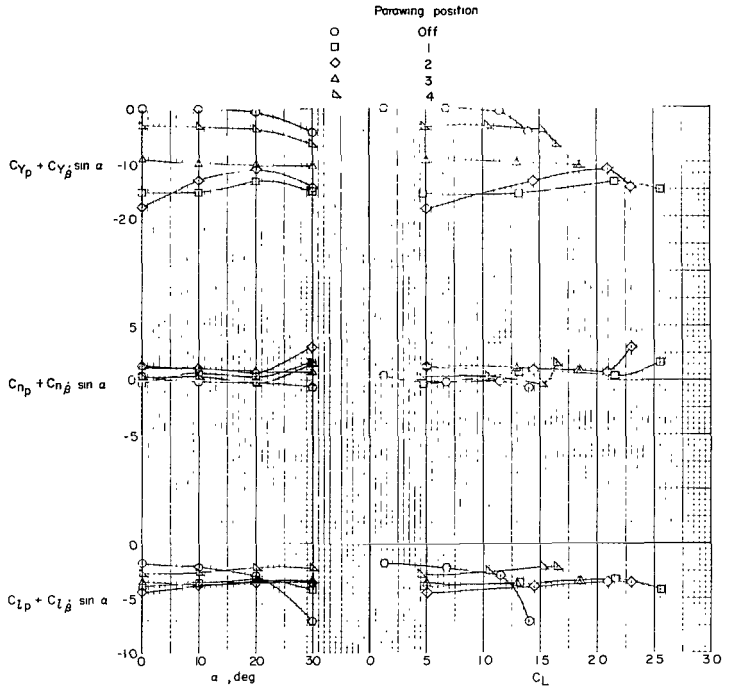

(a) Out-of-phase rolling derivatives.

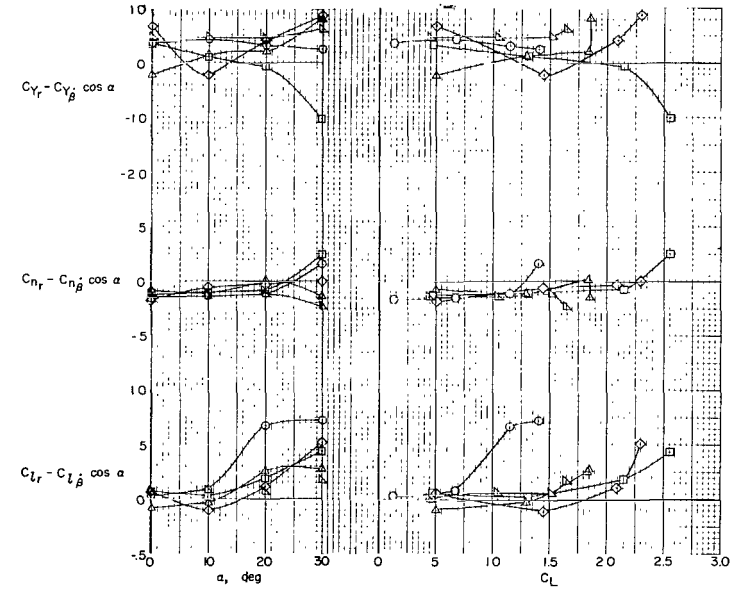

(b) Out-of-phase yawing derivatives.

Figure 15.- Effect of the parawing on the out-of-phase lateral oscillatory derivatives of the model.

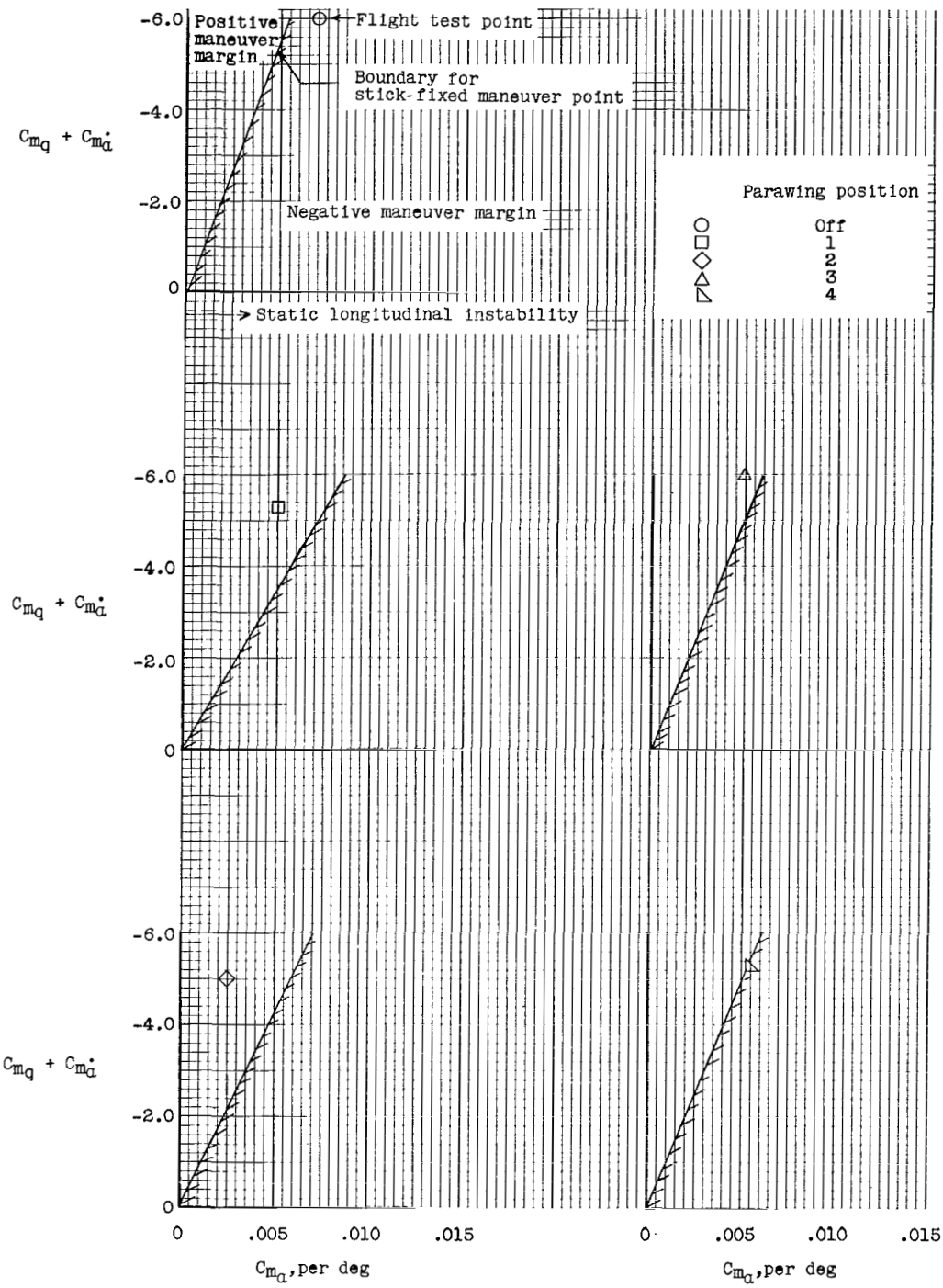

Figure 16.- Effect of damping in pitch and static longitudinal stability on the longitudinal flight characteristics of the model. $\alpha = 20^\circ$; $\delta_e = -10^\circ$.

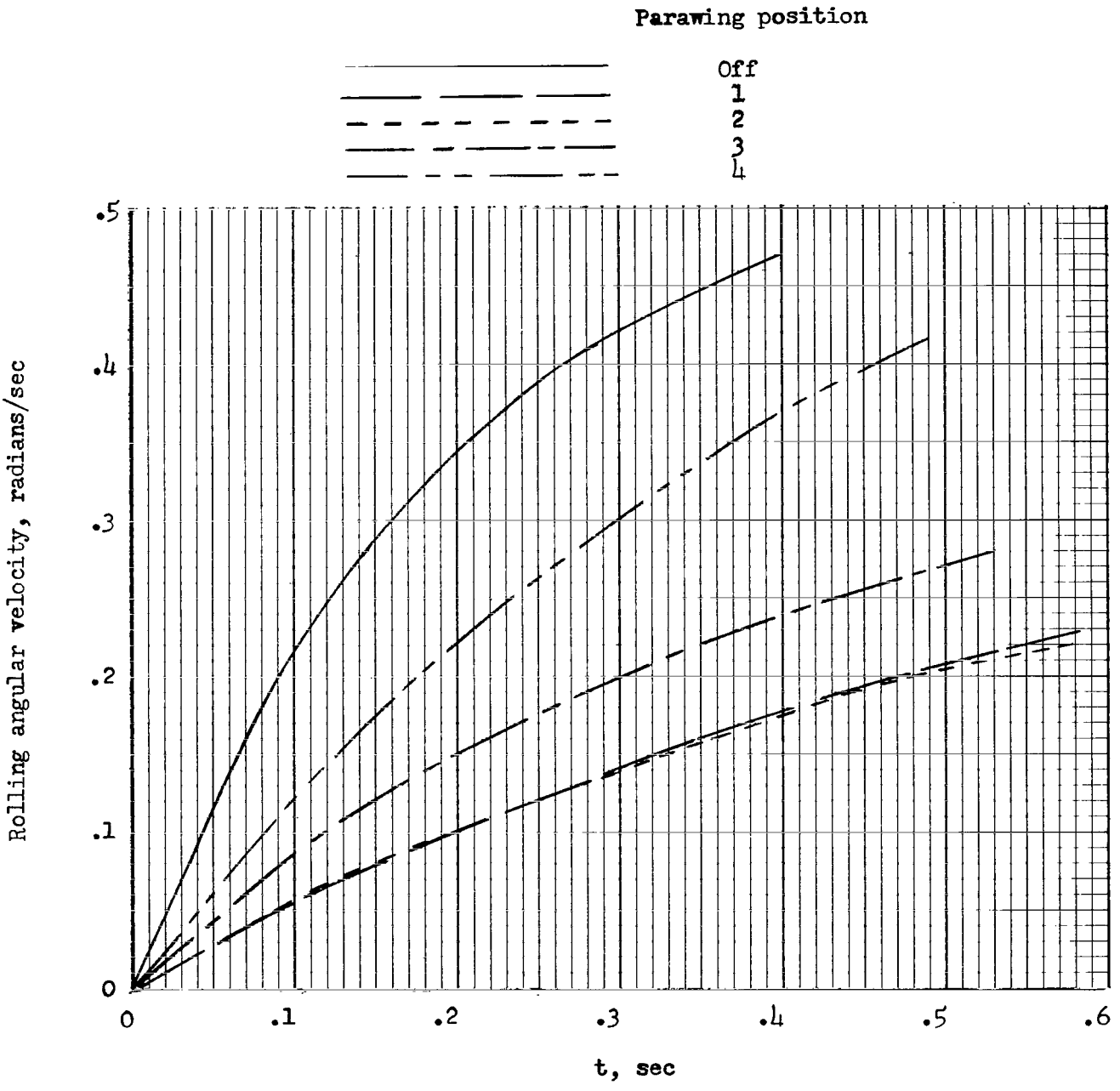

Figure 17.- Effect of the parawing on the calculated rolling response of the model after a constant disturbance input in roll of $\Delta C_l = 0.01$. $\alpha = 20^\circ$. (Calculations were based on freedom in roll only.)